University of Southern Queensland

Faculty of Health, Engineering and Sciences

Behaviour of GFRP Reinforced Concrete Slab on Ground

A dissertation submitted by

Andrew Rayner

In fulfilment of the requirements of

ENG4111 and ENG4112 Research Project

Towards the degree of

Bachelor of Civil Engineering with Honours

Submitted 7th October 2022

Abstract

Concrete replacement and repair costs the Australian economy an estimated $13 billion yearly. Therefore, a more sustainable and durable material is needed especially in coastal and marine environments. Glass fibre reinforced polymer (GFRP) is becoming recognised as an alternative to steel reinforcement with its use overseas. However, Australian engineers and workers have limited knowledge on the handling and construction processes of GFRP-reinforced concrete structures. To develop more knowledge on GFRP this study covers the construction of the approach concrete slabs located at the Mooloolaba boat ramp. The construction involved two different sized reinforcing bars to allow for time and motion analysis. Two slabs were constructed with D24 bars spaced at 300 mm centres each way and two slabs reinforced with D16 bars spaced at 150 mm centres. On-site loading and performance tests were then conducted to provide knowledge on how the on-ground concrete slab performs also allowing validation of a finite element model. Results from the time and motion investigation are highly dependent on the skill level of the workers. This is shown as the efficiency level of the inexperienced workers range from 33-55% when compared to the skilled experienced workers. The D24 and D16 reinforcement required 190.7 and 309.9 worker minutes respectively, therefore indicating that the D16 required 1.6 times longer to construct. Results from onsite loading indicate the largest deflection of 0.144 mm recorded with in the D16 reinforced approach slab (slab P2). P1 (D24 reinforcement) showed deflection of 0.121 mm, therefore showing ≈ 15% less deflection then P2. The finite element model developed in Strand7 software was able to derive the subgrade modulus of the supporting soil beneath the concrete slabs. The modulus of the subgrade beneath P1 was 93 000kN/m^2/m and 115 000 kN/m^2/m for P2. These values correspond to crushed stone with sand, as a 75 mm layer of crushed stone was used to stabilise the sandy subgrade. The parametric investigation discovered that the strength of subgrade modulus was the main variable when considering strain and deflection. The deflection and strain both decrease linearly as the subgrade modulus increases from 80 000 kN/m^2/m, therefore values under this are not recommended. Concluding with the larger spacings in slab P1 have shown to perform better when varying the material parameters, little to no change was seen in deflection while varying bar diameter. As concrete compressive strength increased, P1 showed slight improvement reducing deflection.

University of Southern Queensland

Faculty of Health, Engineering and Sciences

ENG4111 & ENG4112 Research Project

Limitations of Use

Certification

I certify that the ideas, designs and experimental work, results, analyses and conclusions set out in this dissertation are entirely my own effort, except where otherwise indicated and acknowledged.

I further certify that the work is original and has not been previously submitted for assessment in any other course or institution, except where specifically stated.

Andrew Rayner

Student Number: [redacted]

Acknowledgments

I would like to take this opportunity to thank all of the university staff, friends, and family that provided guidance and assisted myself in the completion of this dissertation. I would like to show special appreciation and acknowledgment to my two supervisors, Professor Allan Manalo and Dr Omar Alajarmeh for the countless hours and support you both have offered over this project. Dr Wahid Ferdous, for all of your technical expertise with Strand7.

Lastly, I would like to thank my wife, Kirrilee for your endless patience and support throughout this year.

Andrew Rayner

Table of Contents

List of Figures

List of Tables

Chapter 1

Introduction

1.1. Background and Problem Definition

Concrete is the most used building material worldwide within the construction industry. As concrete is very weak in tension the need for a reinforcing material to carry the tensile loads is required. The most common material since the 19th century is steel due to its high strength and cost effective benefits (McCartney 2017). Although steel is highly vulnerable to corrosion and rust causing major structural problems. Multiple methods can be used to limit corrosion such as increased concrete cover, cathode and sacrificial anode protection, lower water-cement ratios and admixtures (Benzecry et al. 2021a). These methods will not eliminate the problem, only delay the corrosion process. Nolan et al. (2021) reiterated that most of the corrosion in bridge substructures is caused from the exposure to seawater within marine and coastal environments. The chloride ions within the seawater diffuse through the concrete cover and initiate the corrosion process (Benzecry et al. 2021a). Currently bridges are designed to have a service life of 100 years before major repairs are needed. Due to harsh marine environments most coastal bridge structures suffer from corrosion causing major repairs to be made at just 30 years of service (Xu 2016). Concrete replacement and or repair costs the Australian economy an estimated $13 billion annually (Manalo et al. 2021a). Therefore, a more sustainable and durable material is needed especially in coastal and marine environment.

The use of fibre reinforced polymer (FRP) used as concrete reinforcement has increased rapidly over the past decade due to its non-corrosive abilities. Almost 300 bridges have implemented FRP reinforcement within the United States (US) and Canada, proving that composite materials can be used. These structures have shown increased service-life, reduced maintenance and proven that FRP is a sustainable option (Nolan et al. 2021). Glass fibre reinforced polymer (GFRP) is becoming recognised as an alternative to steel reinforcement with its use overseas (Emparanza et al. 2022). GFRP offers various mechanical advantages when compared to steel such as increased tensile strength, one quarter lighter, non-magnetic and does not corrode (Emparanza et al. 2022). Therefore, offering extended durability and reducing the need for maintenance.

Salan et al. (2021) recently completed a comparative case study on the largest GFRP reinforced concrete structure in the world. The structure is designed to mitigate flood waters through a 21 km concrete channel. Originally designed to include epoxy coated steel (ECS) bars as reinforcement. Due to the harsh desert conditions the channel was redesigned to use GFRP bars which increased the design life by an additional 50 years with no maintenance expected. Salan et al. (2021) also compared the cost for the original design to the new GFRP design. Results show a total initial cost saving of $7393 just in materials. Further case studies from Benzecry et al. (2021a) reveal life cycle costs of fibre reinforced concrete achieve 25% lower life cycle costs compared to steel RC. The GFRP RC piles allowed for a 100-year design life in a highly corrosive environment. Manalo et al. (2020a) recently conducted research on precast concrete boat ramp planks utilising GFRP and galvanised steel reinforcement. This showed that less labour and equipment were required when using the GFRP while showing improved structural performance.

Over 30 years of field applications of GFRP reinforcement in bridge structures, has proven to be reliable and increase service life (Nolan et al. 2021). Almost 300 bridges have been completed throughout Canada and the US proving resilience. Although there is still minimal implementation of GFRP reinforcement within Australian structures. Therefore, to increase knowledge around GFRP this research focuses on how slabs perform on ground. This study will aim to investigate the performance of GFRP reinforced concrete slabs in a marine environment, using time and motion recordings, performance loading data and finite element analysis to validate results.

1.2. Research Significance and Project Scope

There is currently no Australian standard for the use of GFRP therefore it is not widely used or accepted but with further results of this study it can support approval. In addition, Australian engineers and workers have very limited knowledge on the handling and construction processes of GFRP-reinforced concrete structures. As multiple studies have proved that GFRP is a viable, long-term solution to replace steel reinforcement, although most published literature has been aimed around suspended slabs and structures.

The scope of this project covers the construction of the approach concrete slab located at the Mooloolaba boat ramp. The construction will involve two different sized reinforcing bars to allow for time and motion to be studied. On-site loading and performance will be conducted to provide knowledge on how the on-ground concrete slab performs also allowing validation of a finite element model. Therefore, finding the optimum reinforcement and subgrade modulus that will ensure sustainable and economical concrete slab design. The complete project specifications and schedule is attached in Appendix A.

1.3. Research Objectives

1. Research the current applications of GFRP and their suitability to reinforce on-ground concrete slabs in marine environments.

2. Conduct a time and motion comparative study on the approach concrete slab construction utilising two different sized reinforcing bars.

3. Investigate the loading performance data gathered from on-site load testing and validate results with finite element analysis.

4. Allow prediction of the optimal reinforcement ratio by utilising finite element software.

   Before commencing this project, a risk management plan (RMP) was completed as shown in Appendix B.

1.4. Dissertation Structure

The structure of this dissertation is broken down into several sections which include 5 chapters, tables, figures, references, and appendices. Below is the layout of each chapter.

Chapter 1:

This section introduced the current problem within the construction industry. While providing information about current alternatives that are already implemented, therefore leading to the objectives scope of this dissertation.

Chapter 2:

This section covers published literature that will define the problem of corrosion within steel reinforcement. GFRP is explored is depth, covering the pultrusion process and the mechanical properties and advantages when compared to steel.

Chapter 3:

The aim of chapter 3 is to document the construction of a GFRP reinforced approach concrete slab in a boating infrastructure project and to investigate the time and motion involved in the construction of the four approach concrete slabs. Results will provide knowledge on the time, labour and different resources involved in the construction of GFRP reinforced concrete structures.

Chapter 4:

This section will investigate loading data collected from site. It will also present the development of a finite element model using Strand7 to predict the behaviour of GFRP reinforced concrete structures. The validated FE model will then be used to investigate the effect of different design parameters including the effect of subgrade modulus on the behaviour of GFRP reinforced concrete approach slabs.

Chapter 5:

This section will conclude the dissertation and will discuss any future work needed towards understanding the performance of GFRP reinforced concrete slabs on ground.

Chapter 2

Literature Review

2.1. Introduction

This chapter of the research is aimed to define the problem of steel corrosion and provide knowledge around glass fibre reinforced polymer (GFRP). The testing methods which are used to determine the mechanical properties of GFRP will be covered below. Also discussed below is the importance of a more sustainable option to reinforce concrete structures.

2.2. Steel reinforcement for concrete

The 19th century uncovered a dramatic innovation by using steel to reinforce concrete structures (McCartney 2017). This allows the compressive strength of concrete to be used while allowing the steel reinforcement to carry the tensile loads. Pushing designing capabilities further by having longer and thinner spans, cantilevered structures, slabs on ground that will carry large amounts of weight while reducing the overall amount of concrete used. The use of steel also helps prevent cracking and shearing while adding to overall strength. Although steel used as reinforcement also has disadvantages leading to unserviceable structures. Moisture enters the concrete through small cracks which leads to an electrochemical reaction. Therefore, allowing an iron transformation into rust, as the rebar rusts the reinforcement can expand up to four times the initial size. Causing cracks and concrete fracture which leads to spalling of the concrete (McCartney 2017). Shown below in figure 2.1 is the effects of the steel reinforcement rusting, causing a spalling action.

Figure 2.1: Reinforcement corrosion (Kodous 2021).

Multiple methods can be implemented to minimise corrosion such as increased concrete cover, sacrificial anode protection, admixtures and increased concrete cover. Although these measures will only delay the corrosion process as the chloride ions which are present in seawater, seep through the concrete cover and initiate the corrosion process (Benzecry et al. 2021a). Currently bridges are designed to have a service life of 100 years before major repairs are needed. Due to saline soils most coastal bridge structures suffer from corrosion causing major repairs to be made at just 30 years of service (Xu 2016). Benzecry et al. (2021b) reiterated that accelerated corrosion rates of up to 500 μm/year can be observed in tidal marine environments.

2.3. GFRP reinforcement for concrete

GFRP bars used as reinforcement within concrete show great potential to eliminate the deterioration within concrete caused by steel reinforcement. The use of GFRP show potential long term benefits such as reduced maintenance costs and increasing the service life. Manalo et al. (2020b) completed a comparative study on the manufacturing and structural performance of boat ramp planks reinforced with GFRP bars and galvanised bars. This study concluded by showing better structural performance when two layers of GFRP bars are used and reduced crack widths when compared to galvanised steel reinforcement (Manalo et al. 2020b).

Chang and Seo (2012) investigated the behaviour of one-way concrete slabs with GFRP reinforcing while comparing the results to steel reinforcement. Multiple slabs were prepared having 13 millimetre diameter GFRP bars for longitudinal reinforcement and two slabs with 16 millimetre steel reinforcement. Chang and Seo (2012) compared under reinforcement and over reinforcement ratios of GFRP and testing with 4-point loading until failure. The aim was to measure performance in terms of deflection, crack pattern and width, ultimate capacity, and failure modes. Results show that the steel reinforced slabs failed due to tensile yielding of the steel bars while the GFRP reinforced slabs failure modes changed with the different reinforcement ratios (Chang & Seo 2012). Under reinforced slabs failed in flexure due to GFRP rupture while over reinforced failed in flexural shear due to concrete failure. Overall the investigation showed that higher reinforcement ratios are needed while designing slabs with GFRP reinforcing, this will then lower deflection and reduce crack widths (Chang & Seo 2012). Sadraie et al. (2019) was in agreement with a higher reinforcement ratio is needed as shown in the impact loading study below.

Sadraie et al. (2019) completed an experimental investigation on the effects of impact loading on concrete slabs reinforced with GFRP. This study was compiled of 15 slabs with various amounts of reinforcement, including plain slabs with no reinforcement, steel and GFRP reinforcement. Test results were achieved by the means of dropping a 105 kg weight from 2.5 metres high, while measuring failure mode, crack development and displacement response. The study found that GFRP will perform better than steel by having a higher reinforcement ratio and adjusting the arrangement (Sadraie et al. 2019).

2.4. Glass Fibre Reinforced Polymer (GFRP)

GFRP is a combination glass fibre-filaments that are longitudinally woven and embedded in a polymer matrix as shown in figure 2.2 (Benmokrane et al. 1995).

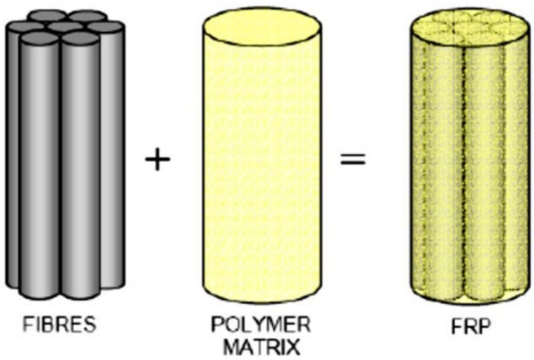

Figure 2.2: Basic material composition of FRP products (Abedini et al. 2017)

The fabrication process involves the extrusion of molten glass fibres through an orifice then soaked in a bonding resin formula before being wound into bar formation, the general process is shown in figure 2.3 (Benmokrane et al. 1995).

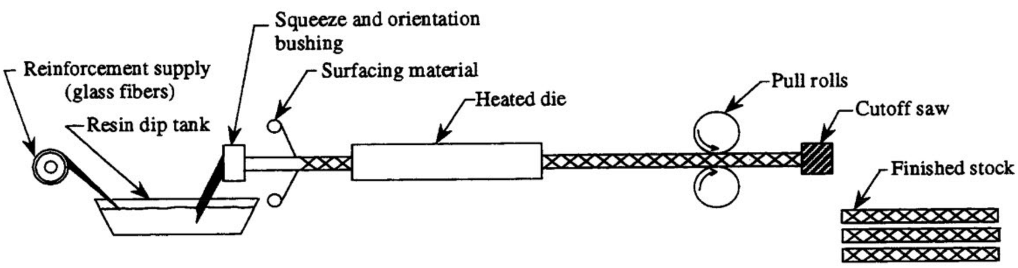

Figure 2.3: Fabrication process of GFRP (Benmokrane et al. 1995).

Glass and Basalt are the most common fibres for the use in rebar although glass is the most common (Emparanza et al. 2017). GFRP has multiple enhanced properties when compared to steel. On average a GFRP bar is one quarter of the weight of steel which will decrease the lifting machinery and man power needed during installation (Emparanza et al. 2017). The main advantages are the non-magnetic and non-corrosive nature of GFRP, even when exposed to harsh conditions like seawater (Emparanza et al. 2017). This section will explain the testing methods used and give insight to why this enhanced product is a more sustainable alternative to steel reinforcement. The properties of GFRP that will be explored below are:

- Bond Strength
- Tensile Strength
- Shear Strength
- Compressive Strength
- Durability

2.4.1. Bond Strength

Multiple studies have been carried out on the use of GFRP in RC, although the first Australian study was published by Gravina and Smith (2008). This study was based on flexural behaviour of indeterminate concrete beams reinforced with fibre reinforced polymer (FRP) rebar. The outcome indicated further investigations were needed as the results were highly dependent on the bond characteristics between the FRP and surrounding concrete. Since then further investigations have been carried out to determine the optimal surface coating to use in reinforced concrete. Yan et al. (2016) collected data from multiple studies containing 682 pull-out-test specimens to observe factors affecting bond behaviour. This study investigated environmental conditions such as freeze-thawing cycles, wet-dry cycling, alkaline solutions, and high temperatures with a combination of different coatings. This resulted in the helically wrapped and sand coated surfaces having the best bond strength discovered from the pull-out test. Shown below in equation 2.1 is to calculate bond strength as specified by ACI 440.1R-06.

$$\frac{\tau_b}{0.083\sqrt{f'_c}} = 4.0 + 0.3\,\frac{C}{d_b} + 100\,\frac{d_b}{l_d} \qquad (2.1)$$

In equation 2.1, τ_b is bond strength (MPa), f'_c refers to concrete compressive strength at 28 day age (Mpa), C is the lesser of the cover to the centre of the bar or one half of the centre to centre spacing of the bars, d_b is the bar diameter and l_d is bedded length Yan et al. (2016).

2.4.2. Tensile Strength

The composition of GFRP allows for a high tensile strength product, Jabbar and Farid (2018) completed a study on GFRP rebar which showed a 13% higher tensile yield strength and 58% higher yield strain. Shown below in Table 2.1 is the comparison of GFRP and steel rebar.

Table 2.1: GFRP vs Steel rebar (Kodous 2021).

	GFRP Rebar	Steel Rebar
Tensile strength (MPa)	>1000	450
Modulus of elasticity (GPa)	>60	190 to 200
Transverse Shear Strength (MPa)	220	300
Bond strength to concrete (MPa)	>20	>12
Ultimate strain %	1.5 - 2%	15%
Density (Kg/m^3)	2100	7800

One of the most common methods to determine the tensile strength of GFRP, is by using a universal testing machine (UTM) (You et al. 2015). The GFRP bar is inserted and centred within a steel tube, the gap between the bar and inner steel wall is filled with a high strength mortar. This process prevents surface damage during the gripping process therefore preventing premature failure. After sufficient curing of the mortar the GFRP bars are then ready to test in the universal testing machine. The tensile strength is determined by the following equation 2.2.

$$f_u = \frac{F_u}{A} \tag{2.2}$$

Where f_u is tensile strength in MPa, F_u is highest amount of load applied before failure in N and A is the cross sectional area in mm^2 Wiater and Siwowski (2020). Shown below in figure 2.4 is the GFRP bar ready to be tested.

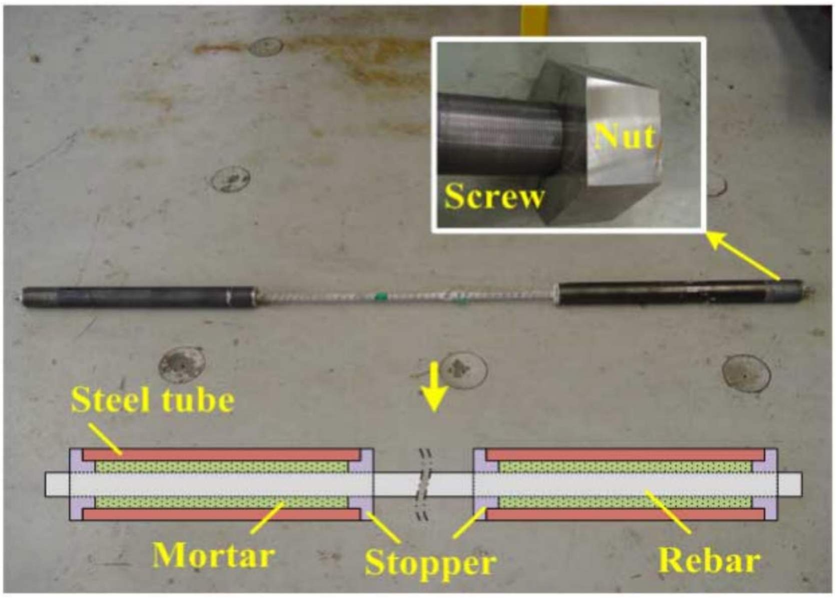

Figure 2.4: GFRP bar ready for tensile testing (You et al. 2015).

Once material is tested in can then be graded, as specific grades are required to allow the use as reinforcement. Table 2.2 below shows the typical mechanical properties with their corresponding grades which are in compliance with the Canadian Standards Association (CSA S-807)

Table 2.2: Typical mechanical properties of GFRP bars (Benmokrane et al. 2016)

Grade	Tensile Strength (MPa)	Modulus of Elasticity (GPa)	Ultimate Tensile Strain
I	588 - 804	40 - 47	0.0134 – 0.0189
II	703 - 938	50 - 59	0.0133 – 0.0179
III	1000 - 1372	60 - 69	0.151 – 0.0211

2.4.3. Shear Strength

The use of GFRP reinforcing has proven to show a decrease in shear capacities when compared to steel reinforcement, which is caused by the low modulus of elasticity within FRP products (Chang & Seo 2012). Chang and Seo (2012) also compared the different shear design standards within the American Concrete Institute (ACI 440.1), Japan Society of civil engineers (JSCE) and Canadians Standards Association (CSA-S806). The results showed that JSCE and CSA-S806 shear equations accurately calculated the shear strength of one-way concrete slabs while using GFRP as longitudinal reinforcement.

2.4.4. Compressive Strength

GFRP bars exhibit a complex behaviour while under compression therefore there is no standard testing procedure for compressive properties (Alajarmeh et al. 2019). Due to the accuracy of current testing methods Alajarmeh et al. (2019) investigated a new compression testing method based on different unbraced bar length (L_u) to bar diameter (d_b) ratios. Figure 2.5 shown below show the testing method and configuration, each sample was tested until failure occurred.

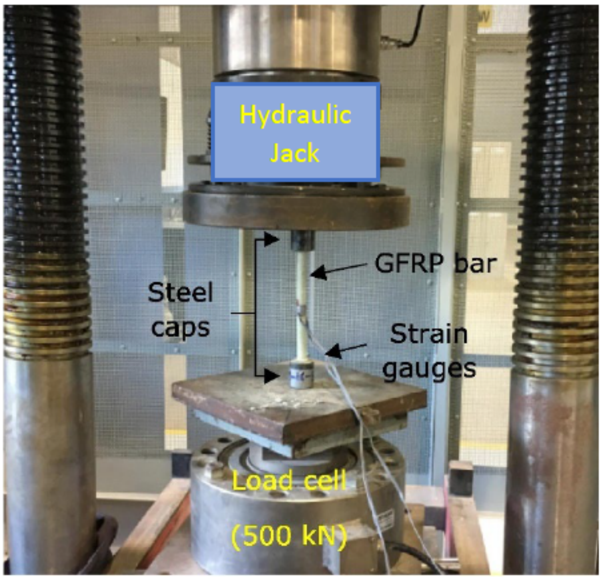

Figure 2.5: Compression testing (AlAjarmeh et al. 2019)

Results indicated a L_u/d_b ratio of 8 gave the most representative value for the compressive strength. The bar diameter did not show any influence on failure mode, although the failure mode can be categorised in accordance with the L_u/d_b ratio. Bars with a ratio up to four failed by crushing, ratios higher than eight failed by buckling and bars with a L_u/d_b ratio between four and eight failed by a combination of crushing and buckling (Alajarmeh et al. 2019). This study gave a better understanding to GFRP under compression which was enforced by the new testing method.

2.4.5. Durability

When GFRP was tested for sustainability characteristics when compared to its steel counterpart by exposing test specimens to one million fatigue cycles (Chu et al. 2020). The testing monitored deflection, stiffness degradation, strains, crack development and the outcome showed enhanced energy absorption, less degradation and improved overall strength with GFRP (Chu et al. 2020). Ramanathan et al. (2021a) conducted a serviceability assessment of GFRP that has been in service for 18 years. Data was gathered via drilling core holes and non-invasive methods such as ultrasonic pulse velocity testing. The outcomes suggested little to no degradation had occurred to the GFRP bars during its lifetime. Ramanathan et al. (2021b) concluded that FRP bars has potential for future construction reinforcement as further studies will enhance the awareness to this non-corrosive material.

Duo et al. (2021) investigated the durability of GFRP when exposed to water, acid and alkali solution at a range of different temperatures to develop a model allowing prediction of tensile strength retention. The research was based on data from 557 experiments on tensile and elastic modulus of GFRP and basalt FRP (BFRP). Results indicated that little to no change in the elastic modulus between the solutions and temperatures. GFRP encountered less degradation within tensile strength when compared to BFRP, this allowed for the new prediction model to be developed as shown below in equation 2.3, equation 2.4 & table 2.3 (Duo et al. 2021).

$$Y = 100exp\left(\frac{-t}{T\phi}\right) \tag{2.3}$$

Y is the strength retention rate, T is temperature in kelvin, t is environmental action time, ϕ is a based on a relationship between solution and temperature given below.

$$\phi = aT + b \tag{2.4}$$

The coefficients for a & b are given in Table 2.3 below along with the confidence level of each value derived throughout the study.

Table 2.3: GFRP coefficients (Duo et al. 2021)

Type of solution	a	b	R^2
water	-0.0064	3.69	0.95
salt	-0.0069	3.86	0.95
alkali	-0.0056	3.51	0.94

Sadraie et al. (2019) conducted research to determine whether the use of GFRP in reinforced concrete slabs would be suitable to withstand impact loading. This was experimental study and verifying the data with finite element software. Results show if the optimal reinforcement ratio could be found with further study, GFRP used in RC would have similar to better performance than steel RC.

2.5. Comparative Studies

Salan et al. (2021) comparative study on the largest GFRP reinforced concrete structure in the world has recently been completed in Saudi Arabia. The structure is a flood mitigation channel 21km long made from reinforced concrete. The original design included epoxy coated steel (ECS) bars to reinforce the concrete which would allow a 50-year service life with only minimal repairs. The harsh corrosive conditions allowed for a strategic redesign which would include GFRP reinforcement. The channels design life was increased to 100 years with no maintenance required. By switching to GFRP less labour and materials where required, therefore saving a total of $7393 for each 30 x 30 m panel (Salan et al. 2021).

Benzecry et al. (2021a) research on the refurbishment of a marine dock with GFRP RC. The comparative study also utilises mixing seawater with concrete instead of fresh water. Results indicate little to no difference with using seawater, and the GFRP reinforcement allows the marine dock to have a design service life of 100-years (Benzecry et al. 2021a).

Manalo et al. (2020a) time and motion studies from the new GFRP precast boat-ramp plank design has given more awareness to the use of GFRP within Australia. This research aimed to collect data of the reinforcement fabrication, formwork setup, installation of reinforcement mesh into formwork, concrete pour, formwork removal and resources required. Three planks where also constructed with the standard galvanized steel reinforcement to have a base point to compare the data. On comparison of the two products GFRP required less labor and equipment and yielded better serviceability and structural performance. This research from Manalo et al. (2020a) has led to the approval and publication the new GFRP plank design for the boating-infrastructure projects within Australia. Manalo et al. (2020a) recommended that further study would confirm that GFRP planks could be fabricated at equivalent cost to steel while having the increased structural performance.

2.6. Concrete construction sustainability

The use of concrete in the construction industry has expanded steadily since the mid-20th century and is not expected to slow down (Scope et al. 2021). Steel has been the most convenient material to reinforce concrete for centuries, due to its mechanical properties ease of accessibility. However this is not a sustainable option, concrete is the most used building material globally and is estimated to cost the Australian economy $13 billion annually for repairs (Manalo et al. 2021b). This excessive amount is based on the steel corrosion within concrete structures. Most bridges that are designed to have a 50 to 100 year life span without repairs, which then lead to major repairs needed at only 30 years of service (Xu 2016). Australia’s harsh coastal environments and aggressive soils makes steel corrosion nearly almost certain.

Precautions can be utilised such as increased concrete cover, stainless steel reinforcement and cathode protection (Manalo et al. 2021b). Although these measures just keep adding to the construction cost making projects uneconomical. Manalo et al. (2021b) concluded that GFRP bars can be as effective as steel reinforcement but incorporates anti corrosion properties. This will allow for slightly higher initial construction cost but less maintenance and extended life spans.

2.7. Summary

This chapter has investigated the problems with steel reinforcement and the published literature on concrete reinforcement alternatives, such as glass fibre reinforced polymer GFRP. The mechanical properties were discussed and how this material is tested and graded. A more sustainable option to reinforce concrete is needed and GFRP shows promising properties. This composite material is already accepted into international concrete standards and has been used in multiple structures. Multiple studies have been completed comparing GFRP to steel reinforcement when used within beams and supported concrete slabs. It can be seen that all have similar results, showing that FRP can perform as an equivalent or higher standard with a higher reinforcement ratio. Therefore, the investigations show that GFRP is the perfect alternative to reinforce concrete and reduce the need for early major repairs in concrete structures. This shows the gap and limited knowledge of how concrete slabs on ground perform and react in harsh marine environments. Further research is also needed comparing the use of different diameters of GFRP bars. Throughout this research the aim is to gain a better understanding of the performance of concrete slabs on ground and how they will perform when loaded. Time and motion will be thoroughly investigated during preparation of boat ramp approach concrete slabs reinforced with two different sized GFRP bars. This will help to identify the best reinforcement to be used with optimal time and machinery savings. The loading data will validate a finite element model which can be used to further predict how the on-ground concrete slabs will perform under multiple loading scenario.

Chapter 3

Time and Motion Studies for GFRP-Reinforced Concrete Slab on Ground

3.1. Introduction

This section will investigate time and motion required to construct four approach concrete slabs at the Mooloolaba boat ramp. The entire construction process has been video recorded to allow the method to be broken down into steps. Focusing on labour, methods and equipment required which will determine activities or materials that can be optimised to save time and cost with construction. Two different sized GFRP reinforcing bars will be used to compare the construction times, and their performance will be analysed in chapter 4 below.

3.2. Slab preparation

Materials and equipment required to prepare the site for slab construction consisted of an excavator, tip truck, temporary fencing, subgrade materials and formwork. The excavator was used to dig out the site and remove the loose sand to allow for sufficient subgrade materials to be installed. The new subgrade consisted of 75 mm of crushed rock with a 50 mm blinder layer of 20 MPa concrete as shown below in figure 3.1. This was designed to ensure a suitable base for the 170 mm thick approach concrete slabs to be laid

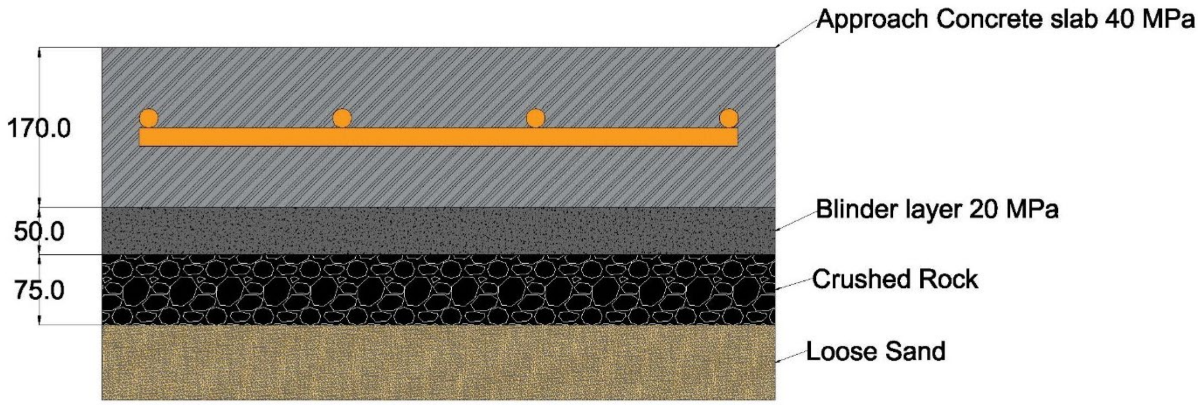

Figure 3.1: Cross section of subgrade preparation.

The excavator was also used to unload the bundles of GFRP bars from a transport truck, this removed the need for a forklift or any other lifting devices. The tip truck was used to transport excavated unwanted fill and then deliver the crushed rock to site. The temporary fencing ensured a safe environment for the public which is required for workplace health and safety regulations. After the blinding concrete layer was cured then the formwork was installed, this allowed for the plastic membrane to be rolled out and the construction of the reinforcing mesh could commence shown below in figure 3.2.

Figure 3.2: plastic membrane installed.

The equipment, materials and labour required in the preparation phase will not be included in the time and motion analysis due to them being common tasks. This will allow for the focus to be on each step in the reinforcement construction.

3.3. Reinforcement Construction

As the GFRP bars arrived on site the initial job was to unload and separate the bars into corresponding lengths shown in figure 3.3. This required the use of the excavator to lift the bundles off the truck and then consumed 139.7 worker minutes to separate into similar lengths. Due to this task being common to all four slabs this will also be excluded from analysis.

Figure 3.3: bundles of GFRP arrived on site.

The four concrete slabs to be poured will be 13 metres long by 4 metres wide having a depth of 170 mm, the concrete will have a compressive strength of $f_c' = 40\ Mpa$. The GFRP bars will be laid with their corresponding centre to centre spacing measurements and tied together with stainless steel wire creating a mesh. The reinforcement will allow 40 mm cover on all edges and will be centred in the slab thickness. The two sizes of reinforcement to be used is D16 GFRP bar with 150 mm centre to centre spacing and D24 GFRP bar with 300 mm centres each way.

The important difference with the D24 slab is the longitudinal bars only have one lap joint as the D16 has two.

To identify differences in the construction of the mesh a process flow chart was derived. The basic symbols and definitions to be used in the flow chart are shown below in Table 3.1.

Table 3.1: Flow chart symbols and definitions.

Flow Chart Symbols		
Symbol	**Indication**	**Definition**
	Operation	Used when performing a task
	Transport	Used when transporting materials
	Repeat	Repeat tasks a certain number of repetitions.

The process has been broken down into multiple tasks which differ slightly with reinforcement size and will be examined in detail below in sections 3.3.1 and 3.3.2 below.

3.3.1. D24 Reinforcement

The D24 GFRP reinforcing bar will be installed to have 300 mm centres each way creating a mesh. The required material is given below:

- 28 longitudinal bars consisting of one lap joint (≈5.6 kg per bar)
- 44 transverse bars (≈5.1 kg per bar)
- Approximately 270 ties

The process consisted of 4 people carrying out tasks, several tasks requiring two people. The tasks involved are shown below in Table 3.2 with the corresponding people required to complete.

Table 3.2: Required number of workers per task.

D24 Construction Tasks		
Task	**Description**	**Required people**
1.	Retrieve longitudinal bars (2 bars)	2
2.	Place longitudinal bars (2 bars)	2
-	Repeat 1 & 2 (total of 14 times)	-
3.	Retrieve one transverse bar	1
4.	Place one transverse bar	1
5.	Tie one transverse bar	2
-	Repeat 3, 4 & 5 (total of 4 times)	-
6.	Place concrete chairs under frame	2
7.	Retrieve transverse bars (3 bars)	1
8.	Place transverse bar (3 bars)	1
-	Repeat 7 & 8 (total of 14 times)	-
9.	Complete tying bars	4
10.	Inspection, mesh adjustment and final chair placement	4

The longitudinal bar retrieval and placement consisted of 2 people carrying an average of 3 bars, this is repeated 9 times until a total of 28 bars are laid. After the longitudinal bars are positioned four transverse bars are installed, one at each end and two evenly spaced only requiring one person. The transverse bars are completely tied in position to create the frame shown below in figure 3.4, then the concrete chairs are placed under the mesh.

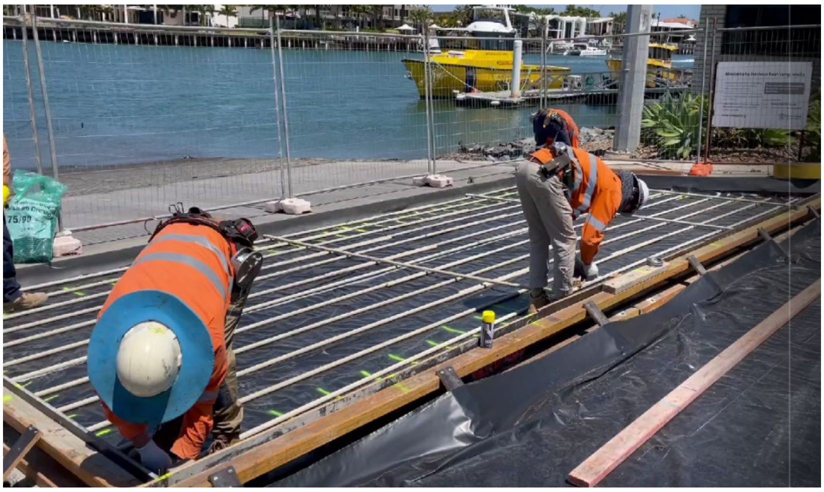

Figure 3.4: D24 mesh frame

Once the frame was sitting on the chairs the remaining transverse bars are installed, this task consists of 2 workers carrying 3 bars each working simultaneously. After the bars are positioned, the transverse bars are completely tied at every second intersection throughout the middle and every intersection around the border. This is the most time-consuming task which required four people working simultaneously. Inspection is carried out for quality control and to reinsure ties have not been missed while readjusting mesh placement if needed. Shown in figure 3.5 below is the completed reinforcement for the D24.

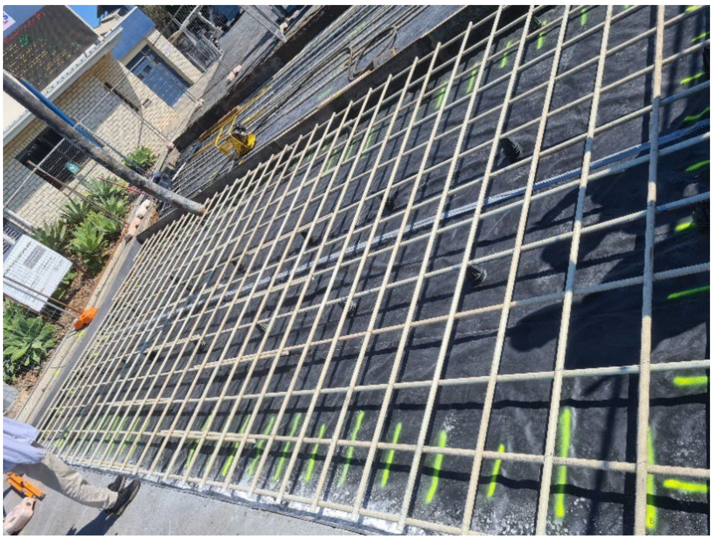

Figure 3.5: D24 mesh complete

The flow chart below in Table 3.3 will show the sequence that each task takes place. The symbol highlighted will indicate each task with an arrow showing how each task in linked.

Table 3.3: D24 construction flow chart.

D24 Construction Flow Chart				
Task	**Operation**	**Transport**	**Repeat**	**Description**
1.				Retrieve longitudinal bars (2 bars)
2.				Place longitudinal bars (2 bars)
-				Repeat task 1 & 2 a total of fourteen times until all 28 bars are laid.
3.				Retrieve one transverse bar
4.				Place one transverse bar
5.				Tie one transverse bar
-				Repeat task 3, 4 & 5 a total of four times until 4 bars laid.
6.				Place concrete chairs under frame
7.				Retrieve transverse bars (3 bars)
8.				Place transverse bar (3 bars)
-				Repeat task 7 & 8 a total of fourteen times
9.				Complete tying bars
10.				Inspection, mesh adjustment and final chair placement.

Throughout the construction process small delays occur slowing the entire process down. The delays are from non-familiarity of GFRP also from less experienced workers waiting for guidance. Due to the number of workers vary with each task, every process is displayed in worker minutes as shown Table 3.4 below.

Table 3.4: D24 construction task time.

D24 Task Times		
Task	**Description**	**Time (s)**
1.	Retrieve longitudinal bars (28 bars)	448
2.	Place longitudinal bars (28 bars)	378
3.	Retrieve 4 transverse bar	60
4.	Place 4 transverse bar	32
5.	Tie 4 transverse bar	1800
6.	Place concrete chairs under frame	1200
7.	Retrieve transverse bars (40 bars)	252
8.	Place transverse bar (40 bars)	196
9.	Complete tying bars (≈ 270)	4080
10.	Inspection, mesh adjustment and final chair placement	1000
11.	Delays	2000
Total	**Seconds**	11 446
	Minutes	190.7

As shown above completing the tying consumes the most amount of time. Delays are expected to reduce with repetition on future projects and familiarity. It is important to note that only the first slab was recorded which has been used for analysis, the second D24 slab would have had slightly reduced construction time.

3.3.2. D16 Reinforcement

The D16 GFRP reinforcing bar will be installed to have 150 mm centres each way creating a mesh. The required material is given below:

- 81 longitudinal bars consisting of two lap joints (≈3.4 kg per bar)
- 87 transverse bars (≈2 kg per bar)
- Approximately 809 ties

The construction process for the D16 reinforcement was slightly more involved as the spacing distance is halved resulting in twice as many bars to be installed. Due to the smaller cross section resulting in a more flexible bar, the method of construction slightly differed from the D24 reinforcement. The construction process involved three workers, 2 experienced workers (worker 1 & 2) and one less experienced (worker 3). This justification has been derived from the average tying and bar retrieval times. Worker 1 was able to retrieve six longitudinal bars each repetition, when compared to worker 3 only carrying two longitudinal bars. The average tying times for workers 1 & 2 are 10.3 and 9.4 seconds respectively when compared to 15 seconds from worker 3. To derive the time and labour for each task the average number of workers are taken from slabs 3 and 4. Shown below in Table 3.5 is the number of workers involved in each task.

Table 3.5: Required number of workers per task.

D16 Construction Tasks		
Task	**Description**	**Required people**
1.	Retrieve longitudinal bars (4 bars)	1
2.	Place longitudinal bars (4 bars)	1
-	Repeat 1 & 2 (total of 7 times)	-
3.	Retrieve end transverse bar	1
4.	Place end transverse bar	1
5.	Tie end transverse bar	2
6.	Retrieve longitudinal bars (4 bars) (2nd row)	1
7.	Place longitudinal bars (4 bars) (2nd row)	1
-	Repeat 1 & 2 (total of 7 times) (2nd row)	-
8.	Retrieve one transverse bar	1
9.	Place one transverse bar	2
10.	Tie one transverse bar and install chairs	2
-	Repeat 8, 9 & 10 (total of 2 times)	-
11.	Retrieve longitudinal bars (4 bars) (3rd row)	1
12.	Place longitudinal bars (4 bars) (3rd row)	1
-	Repeat 11 & 12 (total of 7 times) (3rd row)	-
13.	Retrieve one transverse bar	1
14.	Place one transverse bar	2
15.	Tie one transverse bar and install chairs	2
-	Repeat 13, 14 & 15 (total of 2 times)	-
16.	Retrieve transverse bars (6 bars)	1
17.	Place transverse bars (6 bars)	1
-	Repeat 16 & 17 (total of 14 times)	-
18.	Complete tying bars	2
19.	Inspection, mesh adjustment and final chair placement	2

The D16 concrete slabs are the 3rd and 4th slab to be constructed, the joint between the D16 and D24 slabs consisted of dowel joints spaced at 300 mm centres as shown in figure 3.6(a). The installation of the dowel joints will not be considered in the time and motion analysis. The important difference with the D16 reinforcement is that it consisted of 3 rows of longitudinal bars which required 2 lap joints. This by itself shows increased construction time as the D24 only had one lap joint. The process starts with installing the first row of longitudinal bars which involved 27 bars per row to be retrieved and placed by one worker. The tying process for the end bar involved 2 workers and did not require concrete chairs as the dowel joints supported this bar. As the end bar was being tied worker 3 retrieved and placed the 2nd row of longitudinal bars. Workers 1 & 2 then installed two transverse bars spaced every 17th bar position and placed chairs beneath the frame shown in figure 3.6(b). This allows for worker 3 to install the 3rd row of longitudinal bars while workers 1 & 2 install the last two transverse bars to create the mesh frame as shown below in figure 3.6(c). Once the frame is complete workers 1 & 2 work simultaneously retrieving and installing 6 transverse bars each repetition as worker 1 commences tying. The boarder will be tied at every intersection and every second intersection throughout the middle of the frame equalling $\approx$ 809 ties. After placing all 87 transverse bars workers 1 and 3 will complete tying. The final inspection is then carried out to verify all required intersections are tied and enough concrete chairs are installed, the complete D16 reinforcement is shown in figure 3.6(d) below.

(a) Dowel joints

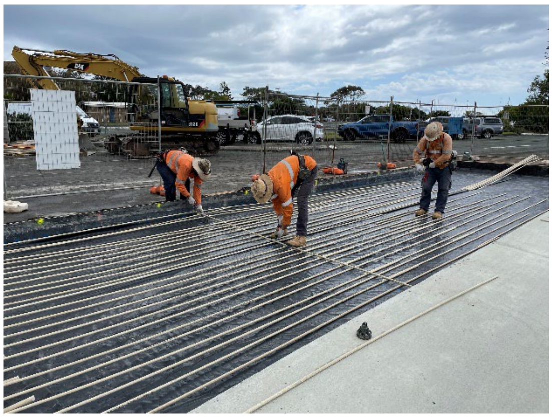

(b) Transverse bar installation

(c) Mesh frame

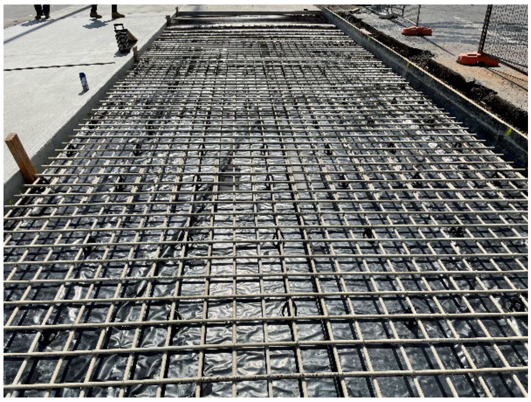

(d) D16 complete reinforcement

Figure 3.6: D16 reinforcement fabrication.

The flow chart below in Table 3.6 will show the sequence that each task takes place. The highlighted symbol indicates the type of activity, the arrow will show how each activity is linked.

Table 3.6: D16 construction flow chart.

Task	Operation	Transport	Repeat	Description
1.				Retrieve longitudinal bars (4 bars)
2.				Place longitudinal bars (4 bars)
-				Repeat task 1 & 2 a total of seven times until 27 bars are laid.
3.				Retrieve end transverse bar
4.				Place end transverse bar
5.				Tie end transverse bar
6.				Retrieve longitudinal bars (4 bars) (2nd row)
7.				Place longitudinal bars (4 bars) (2nd row)
-				Repeat 6 & 7 a total of seven times until 27 bars are laid. (Completes 2nd row)
8.				Retrieve one transverse bar
9.				Place one transverse bar
10.				Tie one transverse bar and install chairs
-				Repeat 8, 9 & 10 a total of 2 times
11.				Retrieve longitudinal bars (4 bars) (3rd row)
12.				Place longitudinal bars (4 bars) (3rd row)
-				Repeat 11 & 12 a total of seven times until 27 bars are laid. (Completes 3rd row)
13.				Retrieve one transverse bar
14.				Place one transverse bar

15.				Tie one transverse bar and install chairs
-				Repeat 13, 14 & 15 a total of 2 times (Note: main frame is complete figure 3.6(c))
16.				Retrieve transverse bars (6 bars)
17.				Place transverse bars (6 bars)
-				Repeat 16 & 17 a total of fourteen times until 82 bars are laid.
18.				Complete tying bars
19.				Inspection mesh adjustment and final chair placement

To derive individual task times, the average activity time has been calculated from slabs 3 and 4 (D16 approach slabs). Several tasks have been combined into similar activities to highlight specific processes that consume the most amount of time. The D16 construction tasks times are shown below in Table 3.7.

Table 3.7: D16 construction task time.

D16 Task Times		
Task	**Description**	**Time (s)**
1.	Retrieve longitudinal bars (81 bars)	382
2.	Place longitudinal bars (81 bars)	550
3.	Retrieve end transverse bar	12
4.	Place end transverse bar	8
5.	Tie end transverse bar	1500
6.	Retrieve middle transverse bars (4 bars)	58
7.	Place middle transverse bars (4 bars)	32
8.	Tie and place concrete chairs (4 bars)	1783.5
	Retrieve transverse bars (82 bars)	361
9.	Place transverse bars (82 bars)	409.98
10.	Complete tying bars (≈ 807)	10 380
11.	Inspection and mesh adjustment	1200
12.	Delays	1500
Total	**Seconds**	18 176
	Minutes	309.94

As shown above in Table 3.7 the complete tying task consumes the largest amount of time. The delays that occurred in the process are from inexperienced workers and non-familiarity of GFRP, this is expected to reduce as future jobs implement GFRP and the workers gain more experience.

3.4. Results

Overall, the 2 different reinforcements consisted of several different tasks through the construction process which are summarised in Table 3.8 below.

Table 3.8: Reinforcement comparison

Reinforcement Comparison		
	D24 (Slab 1 & 2)	**D16 (Slab 3 & 4)**
Centre spacings (mm)	300	150
Total longitudinal bars	28	81
Longitudinal lap joints per bar	1	2
Transverse bars	44	87
Approximate ties	270	809
Worker minutes to complete tying	68	173
Number of Longitudinal bars per repetition	2 workers carry 2 bars	1 worker carries 4 bars
Number of Transverse bars per repetition	1 worker carries 3 bars	1 worker carries 6 bars
Number of Tasks	10	19
Total Time (minutes)	190.7	309.9

As shown one worker can carry twice as many D16 longitudinal bars when compared to two workers carrying 2 pieces of D24 bars. Similar with the transverse bars one worker can carry twice as many D16 then D24 bars. Although the D24 worker minutes required to construct the reinforcement is $\approx$ 1.6 times faster than the D16.

The tying task consumes the most time with both bars, therefore the D24 reinforcement requires 539 less ties which is a major difference. The larger cross section of the D24 bars allowed the complete frame to be assembled before installing chairs. Therefore, the D16 required a slightly different approach as the bars are quite flexible. The D24 required significantly less time to construct therefore, being the optimal reinforcement to be used when only concerned about time constraints. Chapter 4 below will compare the structural performance of the two reinforcements when loaded.

3.5. Discussion

It is important to note that the experience of workers contribute to construction times significantly. As the D24 reinforcement was constructed by 3 experienced workers and 1 less experienced (worker 4). Worker 4 had an average tie time of 17.3 seconds, when compared to the 3 experienced having an average of 9.5 seconds giving worker four a 55% efficiency rate. Another important observation with the D24 construction is that 2 workers were carrying 2 longitudinal bars (≈11.2 kg) and one worker could carry three transverse (≈15.4 kg). Previously 2 workers would be required to carry steel bars however the GFRP bars are lighter so this practice could change and has continued simply via habit. The workers eventually adapted after laying the longitudinal as one worker continued to lay 3 transverse by themselves.

Observations taken during the D16 reinforcement construction highlighted that the less experienced worker (worker 3) was retrieving/placing longitudinal bars at a 33% efficiency rate. As the experienced worker (worker 1) could carry 6 a time (≈12 kg) compared to 2 bars (≈4 kg) by worker 3. The tying efficiency rate from worker 3 was 68% when comparing to worker 1 and 2.

Tables 3.9 and 3.10 below compare experienced workers only verse all workers with the D16 and D24 reinforcement. This will highlight the effect that experience workers have over the less experienced. The longitudinal retrieval and placement times would reduce, and there are no delays although the biggest time saving is in the tying procedure.

Table 3.9: D24 construction with experienced workers.

D24 Reinforcement					
Task	**Description**		**All workers**	**Experienced workers only**	**Time saved**
1	Retrieve longitudinal bars (28 bars)		448	224	224
2	Place longitudinal bars (28 bars)		378	196	182
9	Complete tying bars (≈ 270)		4080	3621	459
Total Time		**Seconds**	11 446	8581	2865
		Minutes	190.7	143	47.7

Table 3.10: D16 construction with experienced workers.

D16 Reinforcement					
Task	**Description**		**All workers**	**Experienced workers only**	**Time saved**
1	Retrieve longitudinal bars (81 bars)		382	212.62	196.38
2	Place longitudinal bars (81 bars)		550	382	168
10	Complete tying bars (≈ 807)		10380	9272.8	1107.2
Total Time		**Seconds**	18176	15231.9	2944.1
		Minutes	309.94	253.9	56.04

As shown the D24 slab is still the preferred choice as the construction time is almost 1.7 times shorter than the D16.

3.6. Recommendations

Further analysis is recommended using an automated rebar tying gun as shown in figure 3.7 below. This tool is proven to have a tie time between 1 - 2 seconds, when compared to an average of 9.5 seconds from experienced workers this would improve productivity substantially. Another option would be to trial the use of zip ties as Manalo et al. (2020b) derived a tie time of 8.37 seconds in the GFRP reinforced boat ramp planks. This also would reduce the overall time, due to the average tie time recorded within the D16 and D24 reinforcement was 12 seconds. The important difference between these projects is that the boat ramp planks are constructed in a controlled environment. As the D16 and D24 reinforcements have been completed on site.

As the unloading and sorting of the GFRP bars where not included within the time and motion analysis. To improve future construction times, it would be recommended that the GFRP be bundled in corresponding lengths before arriving on site as the sorting time consumed 139.7 worker minutes.

Figure 3.7: Rebar tying gun (Madewell products)

Chapter 4

Behaviour of GFRP-Reinforced Concrete Slab on Ground

4.1. Introduction

This section will cover the strain and deflection results while under static and dynamic loading. The load was applied by a water truck with a GVM of 16 tonnes, applying approximately 5 tonnes at each rear wheel and 3 tonnes on each front wheel. The data obtained from site will be compared to a finite element model developed in Strand7 software to verify results. The model will be then used to perform a parametric investigation with different subgrade materials, bar diameters and concrete strength.

4.2.1. Site Performance Evaluation

To analyse the slab performance multiple strain gauges were fitted to the longitudinal bars in slab P1 which was D24 bars spaced at 300 centres and slab P2 with D16 bars spaced at 150mm centres. Unfortunately, several gauges received damage during the pouring and curing process leaving 2 working gauges within slab P1 and 3 in P2. Additional strain gauges were fitting to the concrete surface to evaluate surface strain which is shown by a star (*). Static loading was performed when the rear wheel of the truck stopped on top of the sensors and dynamic loading involved the truck reversing over the slab without stopping. To gather sufficient data the wheels of the truck aligned with the two load paths L_{P1} and L_{P2}. To obtain deflection results a technique called digital image correlation (DIC) was used. The DIC technique is a non-contact optical technique which is used for measuring displacement (McCormick & Lord 2010). Shown below in figure 4.1, 4.2 and 4.3 is strain gauge and load path locations, high-performance DIC camera and the water truck used for loading respectively.

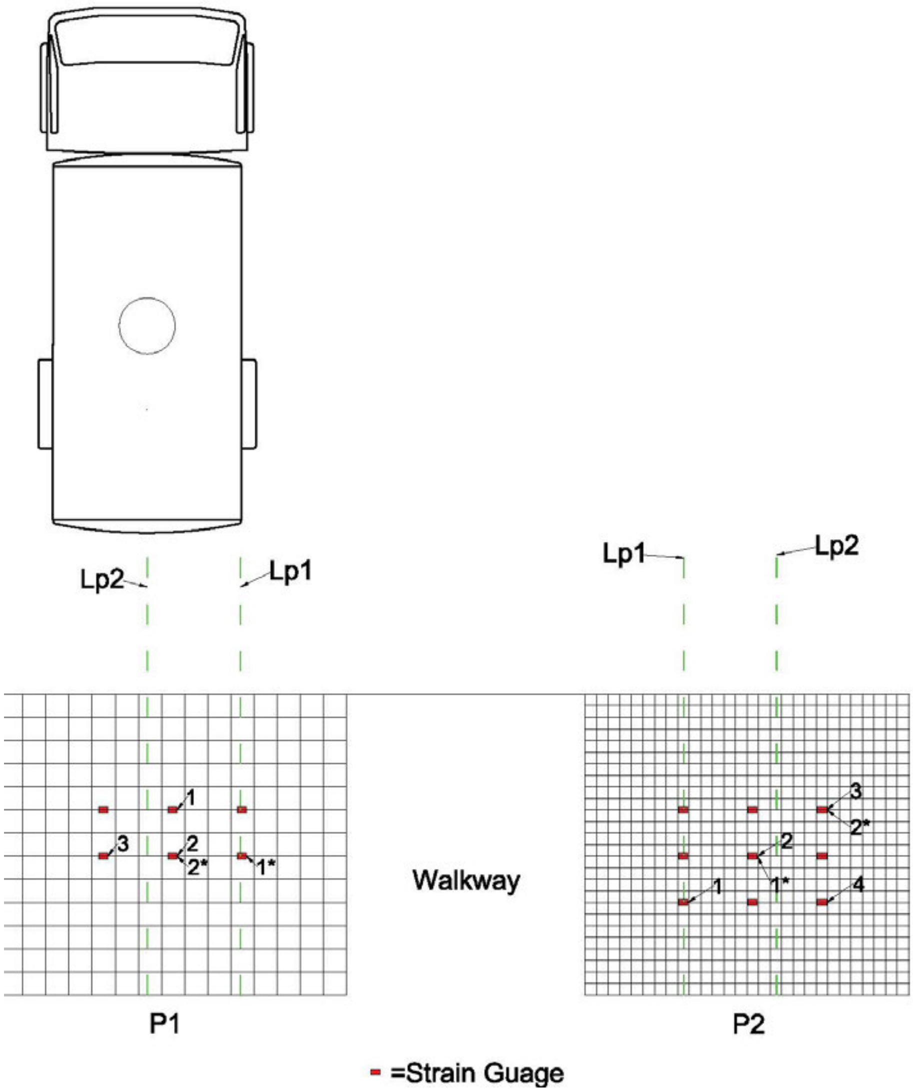

Figure 4.1: Strain gauge and load path locations.

Figure 4.2: High-performance DIC camera

Figure 4.3: Water truck

Result Acronyms are given below:

- P1 = Slab 1 reinforced with D24 bars at 300mm centres each-way.
- P2 = Slab 3 reinforced with D16 bars at 150mm centres each-way.
- L_{P1} = Load path one.
- L_{P2} = Load path two.
- Static loading is taken when the rear wheel is stopped at position 1* delivering 5 tonnes of vertical load at each rear wheel.
- Dynamic loading consists of the truck crossing the slab without stopping.
- SG = strain gauges mounted on the longitudinal bars embedded in the concrete.
- * = strain gauges mounted on top of the concrete to measure surface strain.

4.2.2. P1 – L_{P1} – Static

Slab P1 with static loading applied along L_{P1} obtained a maximum reading on the surface at SG1* of 79 micro strain ($\mu\varepsilon$). The maximum strain reading measured on the reinforcing bars was 55 $\mu\varepsilon$ at SG1, located between the back wheels. Shown below in figure 4.4 is the resulting strain curve for approach slab P1 along load path L_{P1}.

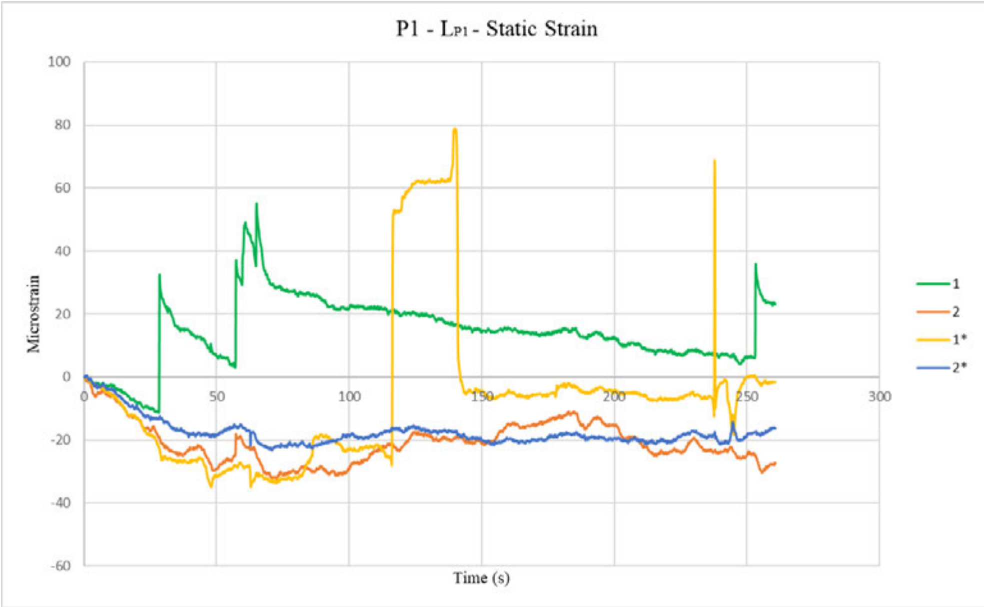

Figure 4.4: P1 – L_{P1} – Static Strain curve.

The deflection readings taken at position 1* which is shown below in figure 4.5.

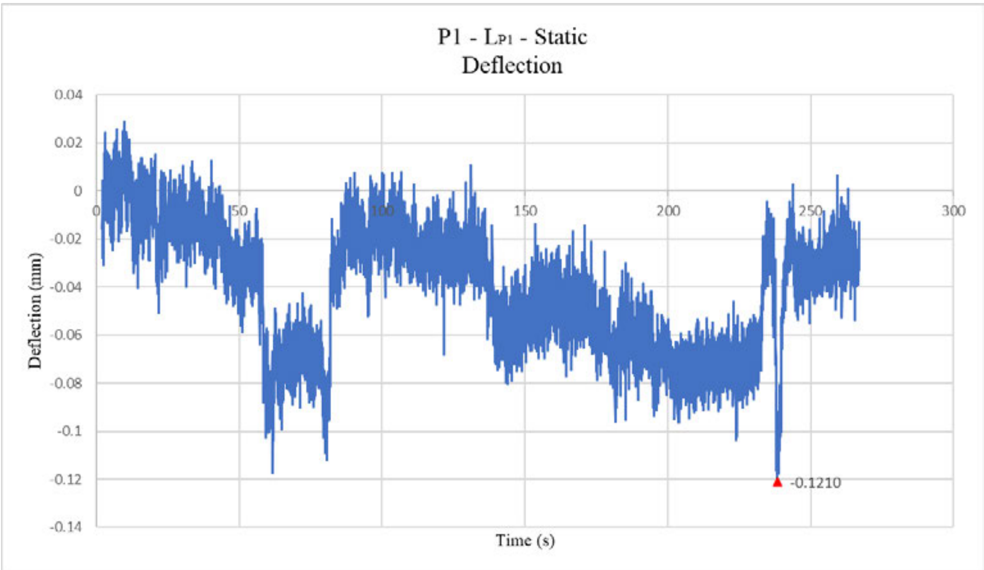

Figure 4.5: P1 – L_{P1} – Static Deflection at position 1*

The initial peak value of -0.11mm deflection between 60 – 80 seconds was when the truck stopped on position 1*. The peak value of -0.121mm as shown above was seen to be when the truck started moving forward off again.

4.2.3. P1 – L_{P1} – Dynamic

The peak strain was also seen to occur on the surface at SG1* measuring 92 $\mu\varepsilon$, the values are shown to peak as the wheels travel over this position. The reinforcing bars show a maximum strain reading of 50 $\mu\varepsilon$ at SG2 as shown below in figure 4.6.

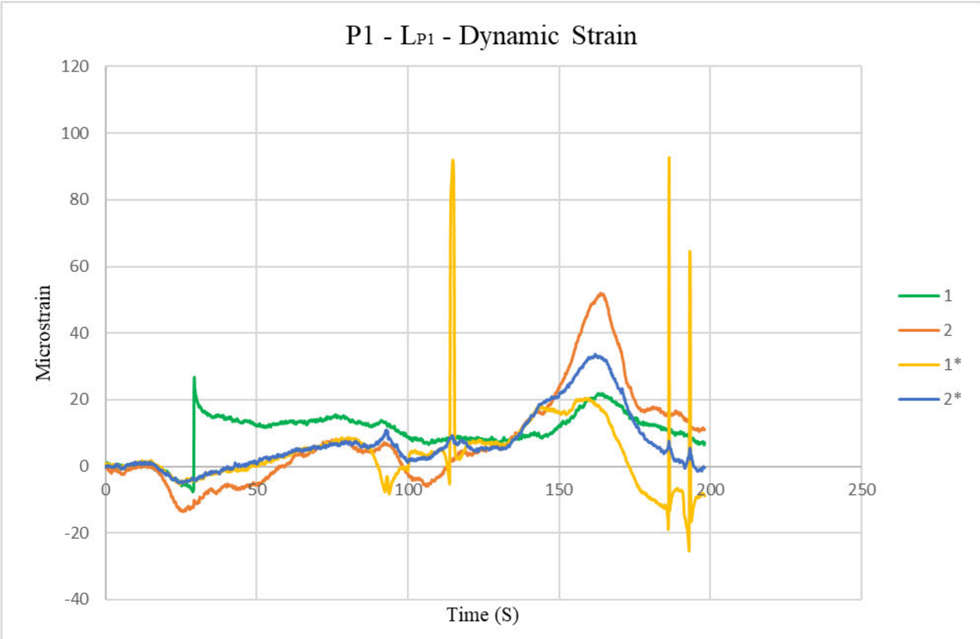

Figure 4.6: P1 – L_{P1} – Dynamic Strain curve.

Shown below in figure 4.7 is the deflection at position 1* under dynamic loading. As shown the peak downwards value of deflection is -0.105mm, this is as the rear wheel passes over location 1*. It can be seen that between 30 – 50 seconds the rear wheel passes over the slab which results in a positive value until the front wheel approaches position 1*.

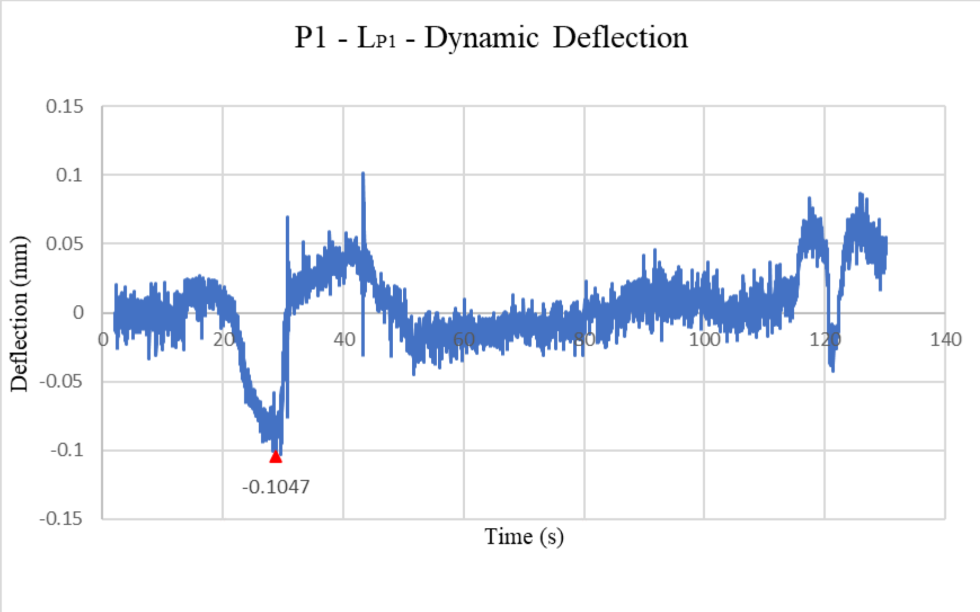

Figure 4.7: P1 – L_{P1} – Dynamic Deflection at position 1*

4.2.4. P1 – L_{P2} – Static

Load path two shows similar results with the peak strain value located on the surface, under the wheel load at SG2* delivering 120 $\mu\varepsilon$. The maximum strain recorded on the reinforcing bars was 52 $\mu\varepsilon$ at SG1 as shown below in figure 4.8.

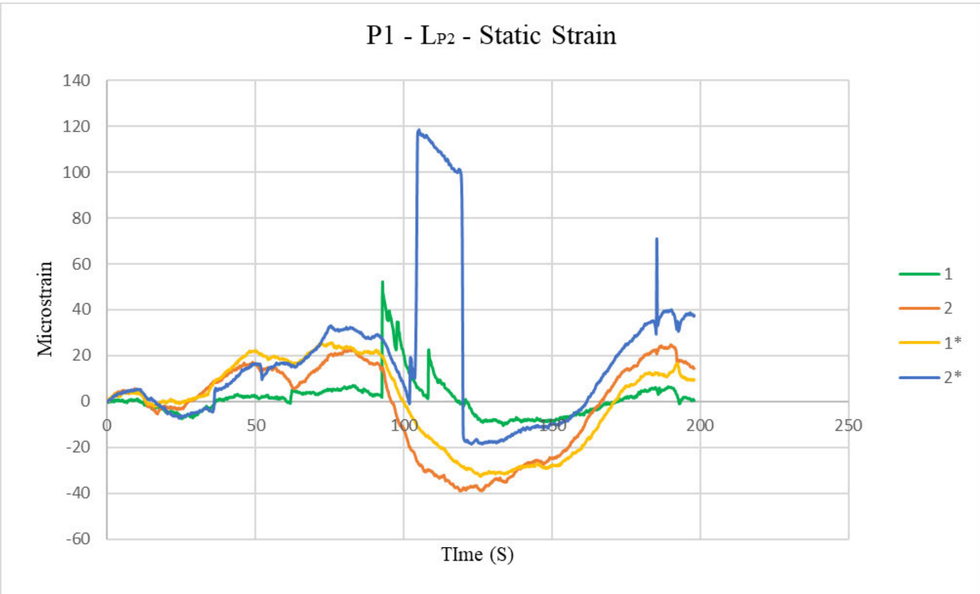

Figure 4.8: P1 – L_{P2} – Static Strain curve

4.2.5. P1 – L_{P2} – Dynamic

The initial peak strain occurs as the truck reverses over SG2*, the highest peak can be seen to occur as the truck drives forward back across SG2* resulting in 230 $\mu\varepsilon$. The highest reinforcing bar measurement was 78 $\mu\varepsilon$ at SG1, as shown below in figure 4.9.

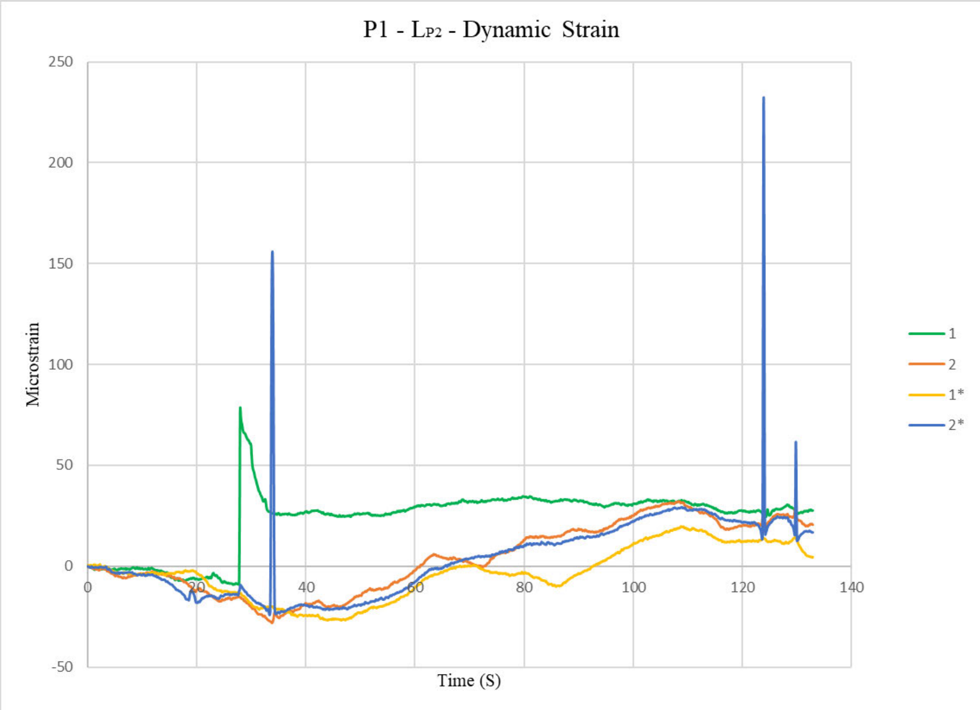

Figure 4.9: P1 – L_{P2} – Dynamic Strain curve.

4.2.6. P2 – L_{P1} – Static

Shown below in figure 4.10 is the static strain recorded at slab P2, it can be seen that the surface strain gauges SG1* and SG2* indicate compressive strain as the wheel is in direct contact showing 95 $\mu\varepsilon$. The reinforcing bars show a stable 28 $\mu\varepsilon$ at SG4 as the truck is stopped. The peak value is recorded as the truck starts to move forward at SG1 measuring 45 micro strain.

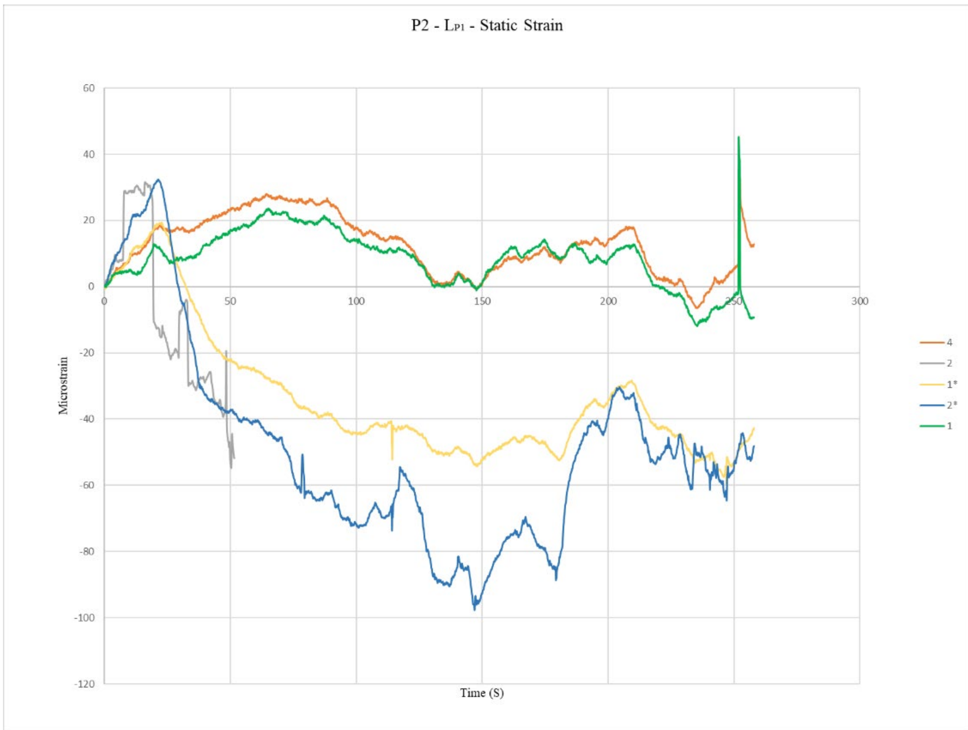

Figure 4.10: P2 – L_{P1} – Static Strain curve

The deflection recorded at position 1 is shown below in figure 4.11. The initial deflection has an average value of -0.067mm downwards as the rear wheel is stopped on position 1. The positive deflection recorded after this was caused from the rear wheel leaving the slab causing a cantilever effect. The deflection is shown to level out between 150 – 240 seconds as the front wheel is stopped on position 1.

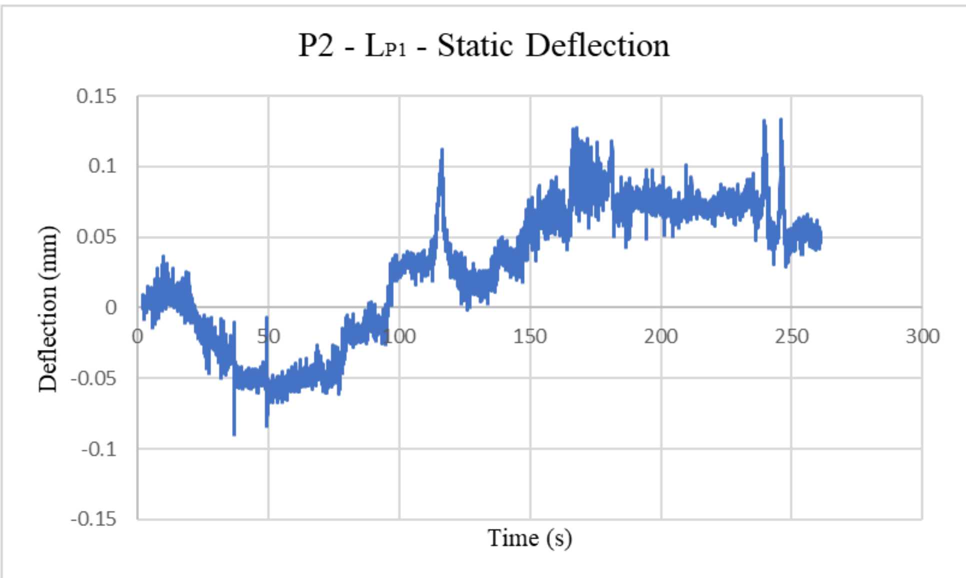

Figure 4.11: P2 – L_{P1} – Static Deflection at position 1

4.2.7. P2 – L_{P1} –Dynamic

Figure 4.12 shown below demonstrates the strain within the longitudinal bars as the truck is moving over the slab. SG1 and SG4 has recorded 18 $\mu\varepsilon$, this occurs as the rear wheel is over position 1. Surface strain is shown to peak while under compressive strain showing values of 115 $\mu\varepsilon$.

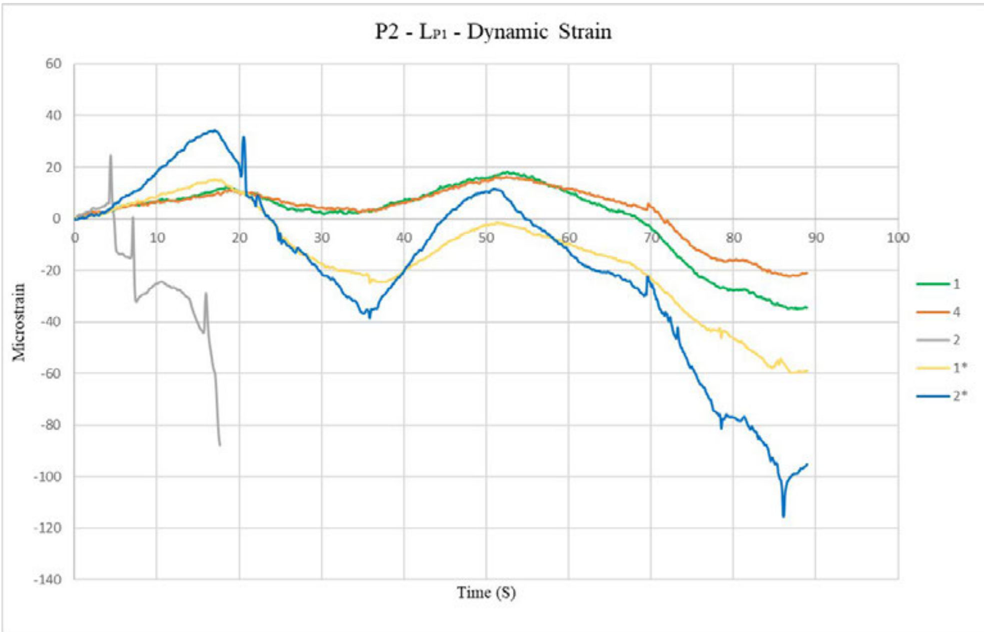

Figure 4.12: P2 – L_{P1} – Dynamic Strain curve

The deflection as demonstrated below in figure 4.13 recorded an initial value of -0.05mm as the rear wheel passes over position 1. The DIC camera has a misreading between 20 and 30 seconds as shown by the positive peak as the rear wheel is over position 1. The value then increases to a positive deflection as the rear wheel leaves the slab causing a cantilever action until the front wheel approaches position 1.

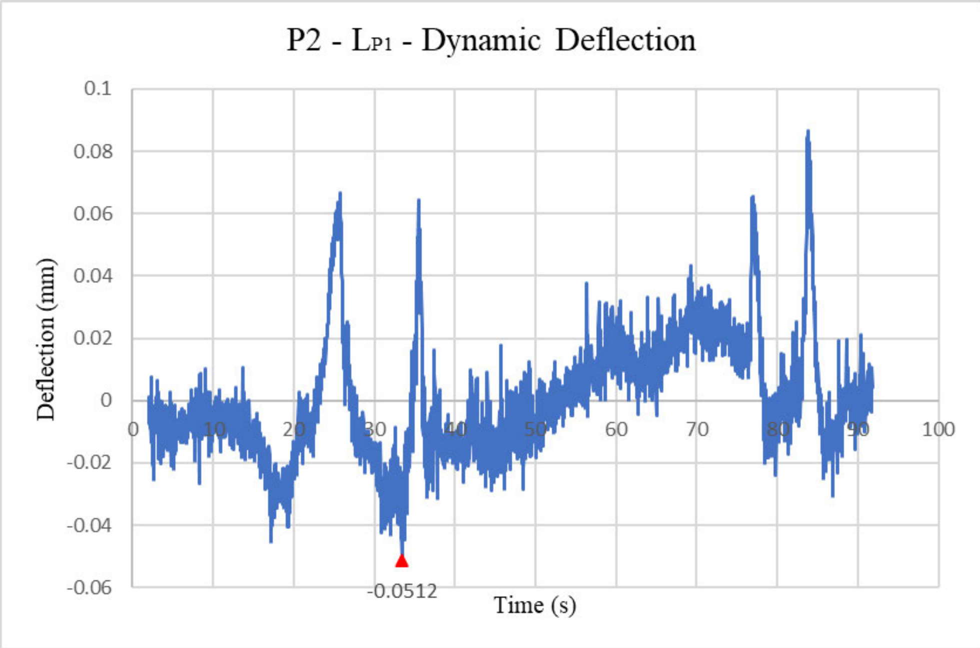

Figure 4.13: P2 – L_{P1} – Dynamic Deflection at position 1

4.2.8. P2 – L_{P2} – Static

The peak value that occurred in the reinforcing bars can be seen below in figure 4.14. This occurred at SG1 with a value of 42 $\mu\varepsilon$, this is observed as the rear wheel is stopped on position 1, while surface strain is seen to peak at 60 $\mu\varepsilon$.

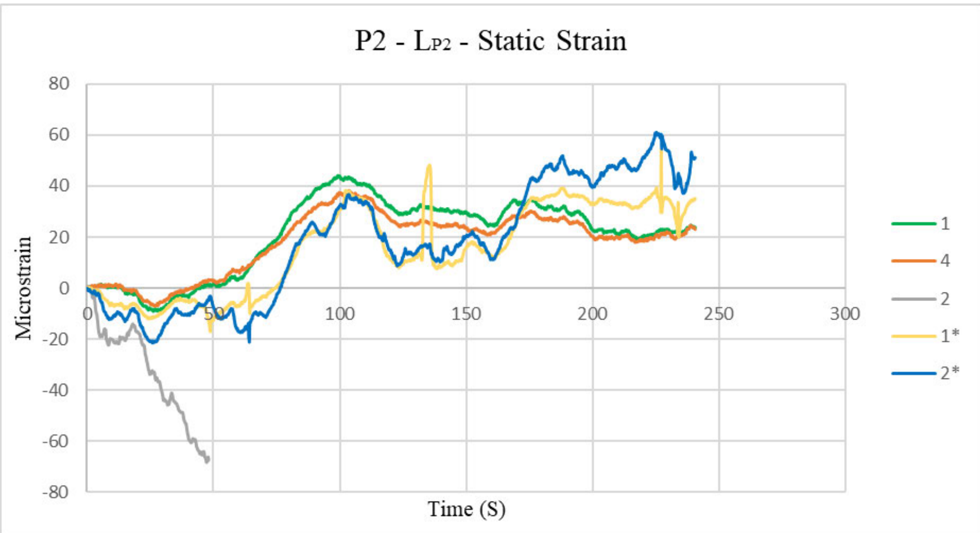

Figure 4.14: P2 – L_{P2} – Static Strain curve

The initial deflection between 10 – 50 seconds occurred when the rear wheel is stopped on position 1. The truck moves backwards causing a positive deflection until the front wheel is positioned on top of SG1 which is between 75 to 120 seconds. The truck then moves forward to reposition the rear wheel which is when the peak value of -.108mm downwards is recorded as shown in figure 4.15.

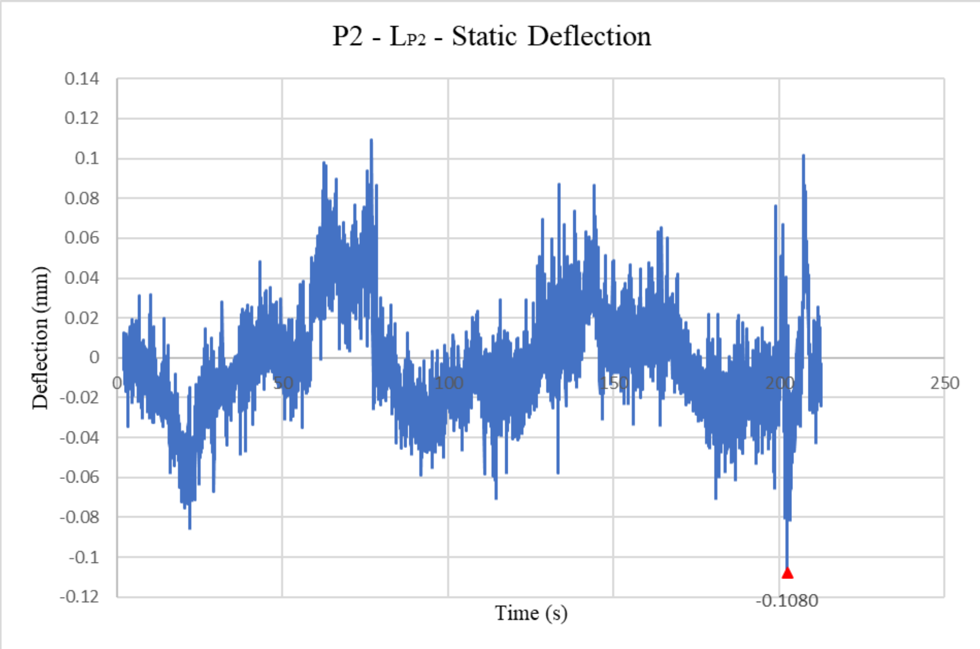

Figure 4.15: P2 – L_{P2} – Static Deflection at position 1

4.2.9. P2 – L_{P2} – Dynamic

Figure 4.16 below demonstrates 10 $\mu\varepsilon$ in SG1, this strain gauge shows the strain developed in reinforcing bars. The surface strain gauges can be seen to peak with compressive strain at 40 $\mu\varepsilon$ as the wheel is directly on top of the gauge.

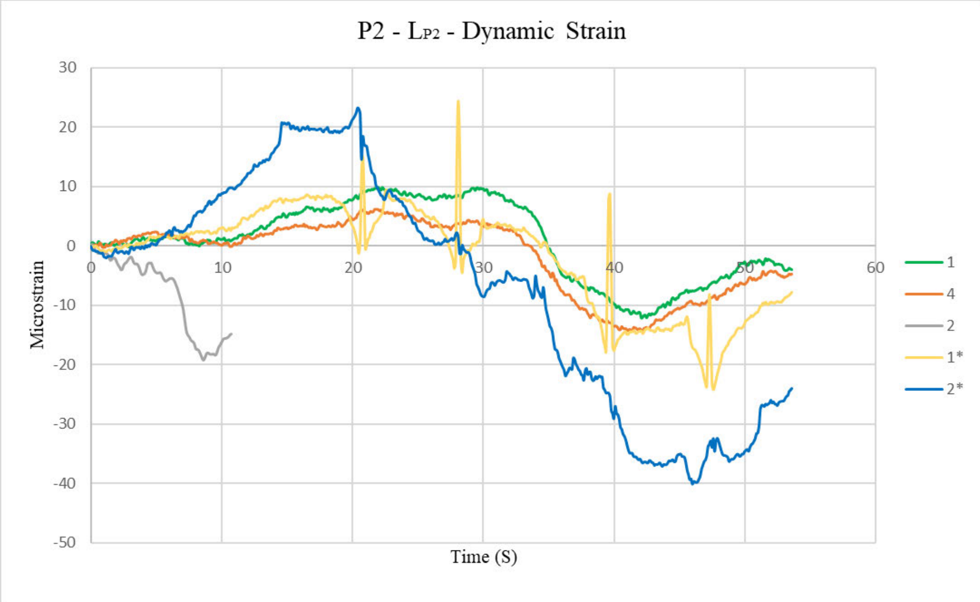

Figure 4.16: P2 – L_{P2} – Dynamic Strain curve

The deflection captured by the DIC camera showed peak deflection of -0.144mm downwards as the rear wheel passes over position 1. Figure 4.17 below demonstrates a similar cantilever effect as the rear wheel passes over the slab.

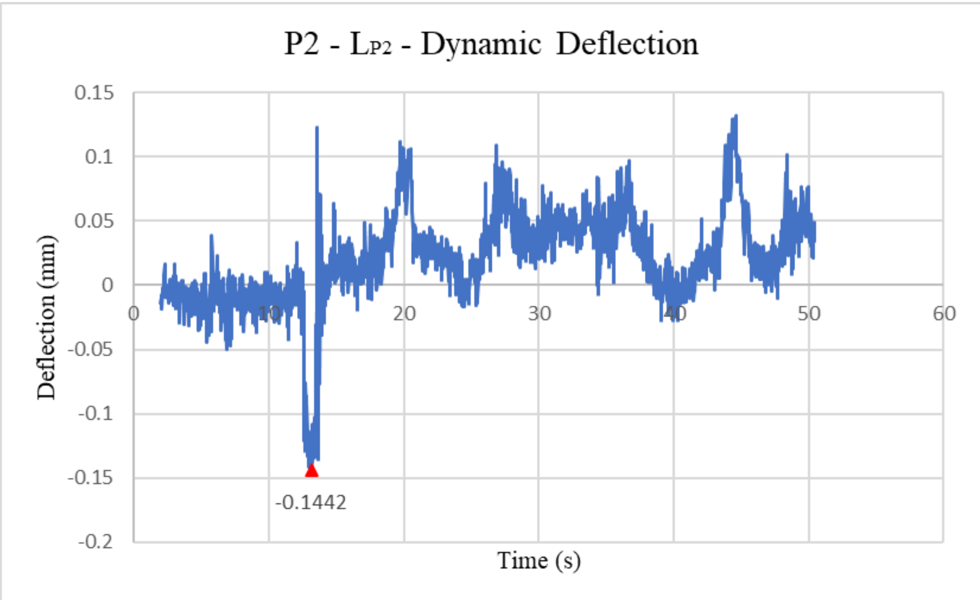

Figure 4.17: P2 – L_{P2} – Dynamic Deflection at position 1

4.3. Finite Element Model

To allow further analysis and investigate how subgrade strengths affect the behaviour of the slab, Strand7 computer software will be implemented. Modelling the concrete slabs will include elastic subgrade modulus to replicate the behaviour of the supporting subgrade. Site measurement included dynamic and static loading, for simplification the model will be using static loading along the 2 load paths. Figure 4.18 below demonstrates the loading configuration to be used for the Strand7 model.

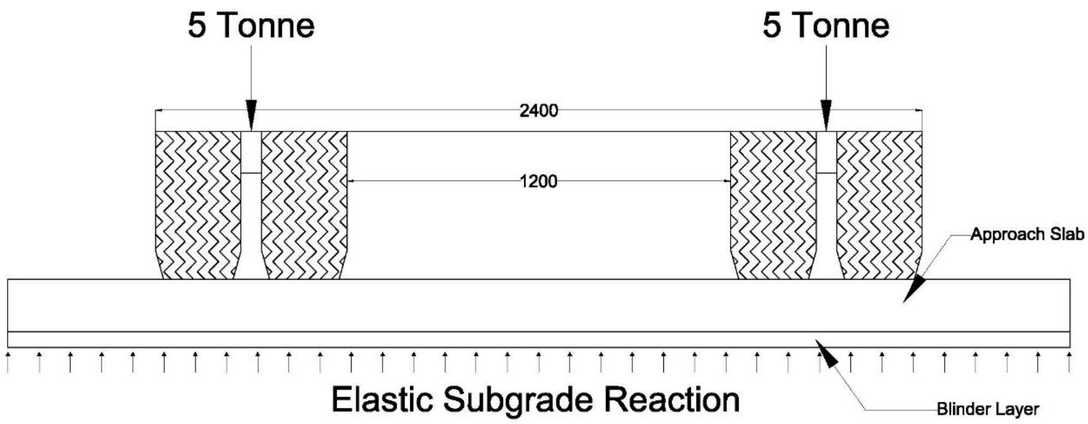

Figure 4.18: Loading Configuration.

The truck tyre footprint size is 300 x 600 mm which applied a uniform pressure of 272.5 kPa to the concrete surface as shown below in figure 4.19.

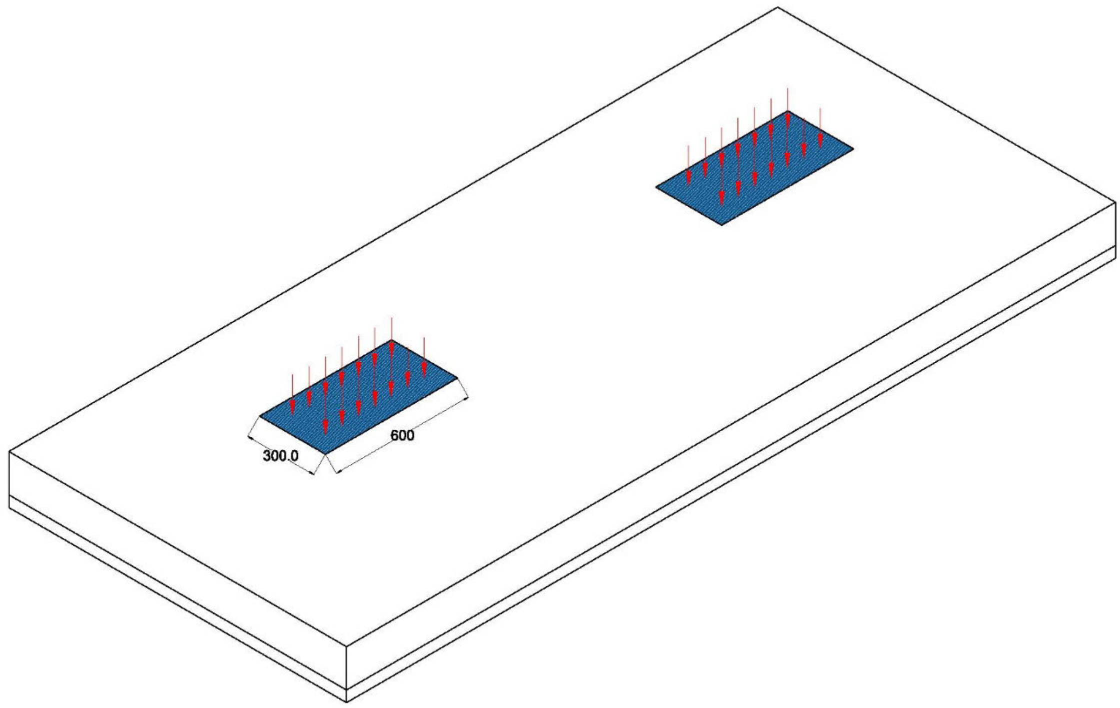

Figure 4.19: Truck tyre contact footprint.

The data inputs used in the finite element software model are shown below:

- Poisson's ratio = 0.25 (Tekle et al. 2017)
- GFRP Density = $2.585 \times 10^{-4}\ kg/\ m^3$
- Approach concrete slab $f'_c = 40Mpa$
- Blinder concrete $f'_c = 20Mpa$

The subgrade modulus can range from 5000 to 300 000 kN/m^2/m depending on soil types and compactness. Due to this large range, the trial-and-error method has been used to identify the subgrade strength beneath the concrete slabs. Table 4.1 summarises the subgrade reactions for different soils.

Table 4.1: Modulus of subgrade reactions for different soils (Uzodimma et al. 2020)

Soil Description	ks (kN/m^2/m)
Humus soil or peat	5000 - 15000
Recent embankment	10000 - 20000
Fine or slightly compacted soil	15000 - 30000
Well compacted sand	50000 - 100000
Very well compacted sand	100000 - 150000
Loam or clay (moist)	30000 - 60000
Loam or clay (dry)	80000 - 100000
Clay with sand	80000 - 100000
Crushed stone with sand	100000 - 150000
Coarse crushed stone	200000 - 250000
Well compacted crushed stone	200000 - 300000

4.3.1. P1 Strand7 Model

Slab P1 is reinforced with D24 bars spaced at 300 mm centres each way, which required 3080 nodes to create a working model. The reinforcing bars are fixed around the entire perimeter of the slab. This replicates the reinforcing being tied to the starter bars, which will ensure a strong connection between corresponding slabs. Shown below in figure 4.20 is the model for slab P1, the red layer on the bottom indicates the 20 MPa blinding layer of concrete.

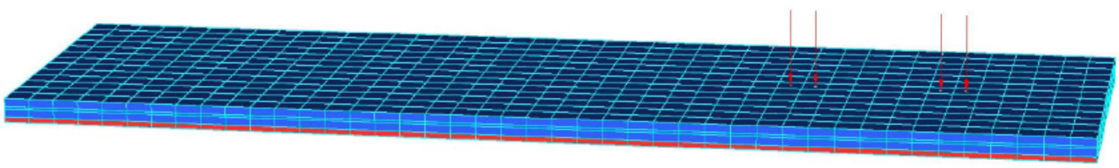

Figure 4.20: Strand7 model of slab P1.

The subgrade modulus used for slab P1 was 115 000 kN/m^2/m, therefore creating a deflection of 0.121 mm in the centre of the slab. These results match the deflection readings that were taken on sight for load path 1 static loading. Shown in figure 4.21 is the finite element model of slab P1 with loading applied demonstrating deflection. Figure 4.22 demonstrates the stress locations in the reinforcing mesh, detailed Strand7 results can be found in Appendix C.

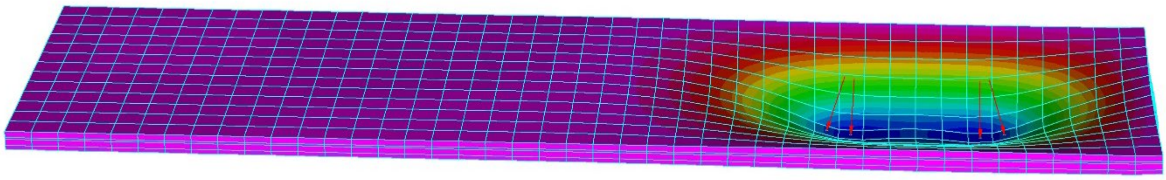

Figure 4.21: Model of slab P1 with loading applied demonstrating deflection.

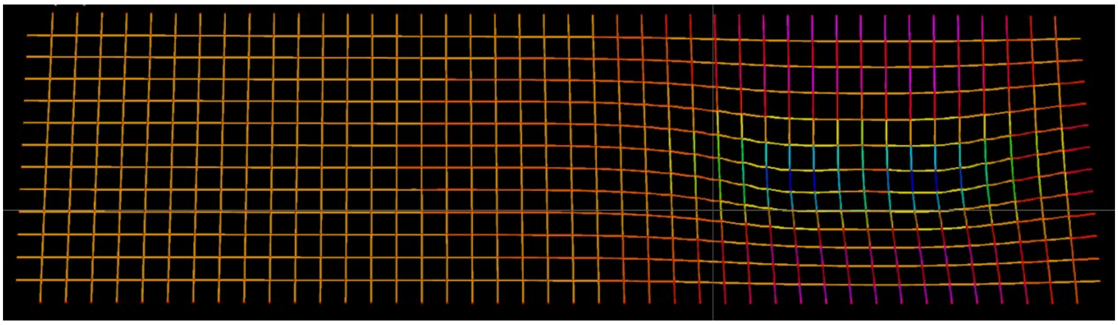

Figure 4.22: Stress concentrations in reinforcing mesh for slab P1

As shown the deflection and stress concentrations are localised around the loading points. The highest stress locations are beneath the wheel loading and stress is also seen around the edges close to the load path. Figure 4.23 below shows a zoomed in area of loading, this clearly shows where the stress is acting. It can be seen that stress is present at the bar ends, this is explained since the ends are fixed and in tension as the load deflects the reinforcing mesh.

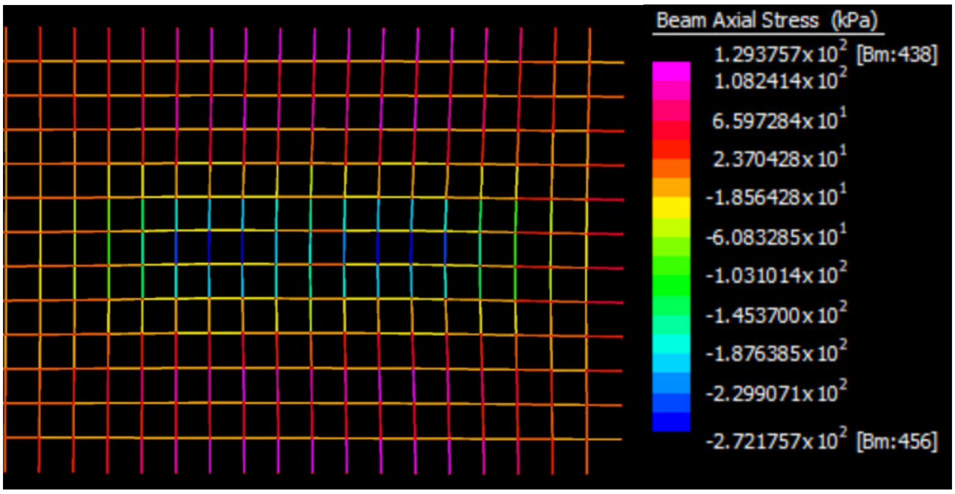

Figure 4.22: Stress in reinforcing mesh slab P1.

Equation 4.1 below is used to convert stress to micro strain.

$$\mu\varepsilon = \frac{\sigma}{E}$$

(Equation 4.1)

Where:

$$\mu\varepsilon = micro\ strain$$

$$\sigma = Stress\ (kPa)$$

$$E = Youngs\ Modulas\ (GPa)$$

The highest value of micro strain present in the reinforcing mesh is 4.53 $\mu\varepsilon$, the highest value recorded from site data was 55 $\mu\varepsilon$. The difference is approximately a factor of 10, this can be caused from incorrect end conditions within the finite element model.

4.3.2. P2 Strand7 Model

Slab P2 is reinforced with D16 bars spaced at 150 mm centres each way, this required 11 745 nodes to create a working model. This slab is also fixed to neighbouring slabs with starter bars, therefore all of the bar ends are fixed to replicate this. Shown below in figure 4.23 is the Strand7 model of slab P2.

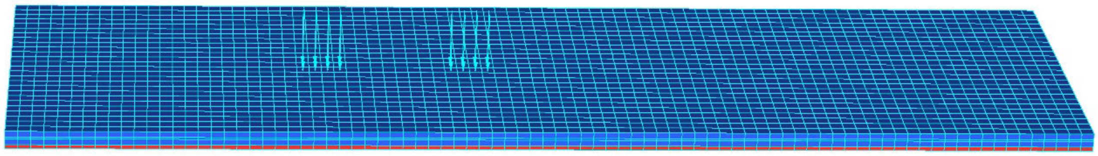

Figure 4.23: Strand7 model of slab P2.

The derived subgrade modulus for slab P2 was 93 000 kN/m^2/m, therefore having a deflection of 0.144 mm in the centre of the slab. This corresponds to the maximum deflection measured on site, this was located along load path 2. The deflection of the slab and stress locations in the mesh can be seen in figure 4.24 and 4.25 respectively.

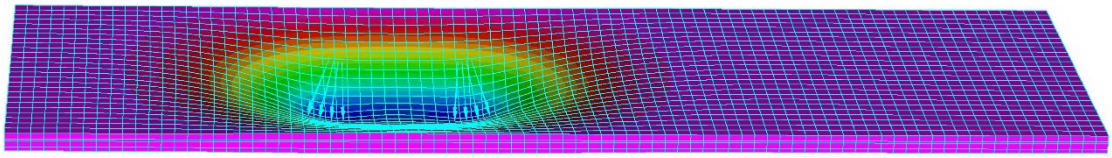

Figure 4.24: Deflection of slab P2 along load path 2.

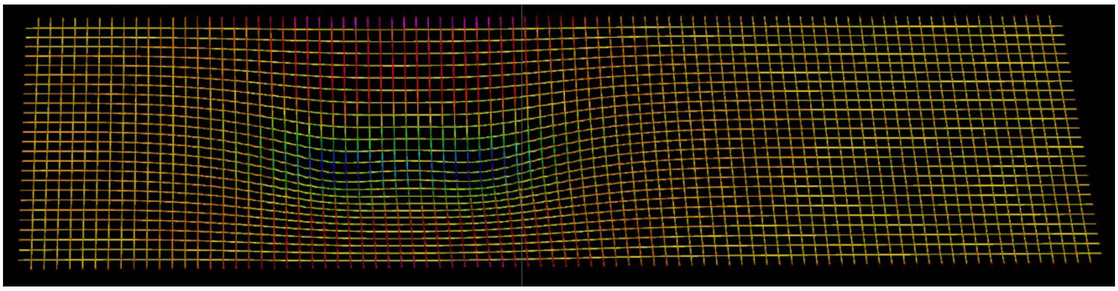

Figure 4.25: Stress concentrations in reinforcing mesh for slab P2

The maximum stress is located directly under the wheel loads as represented by the blue area shown below in figure 4.26. Slab P2 showed a value of 42 $\mu\varepsilon$ derived from site measurements when compared to the model showing 5.26 $\mu\varepsilon$. The cause of this discrepancy is most likely the end conditions within the model.

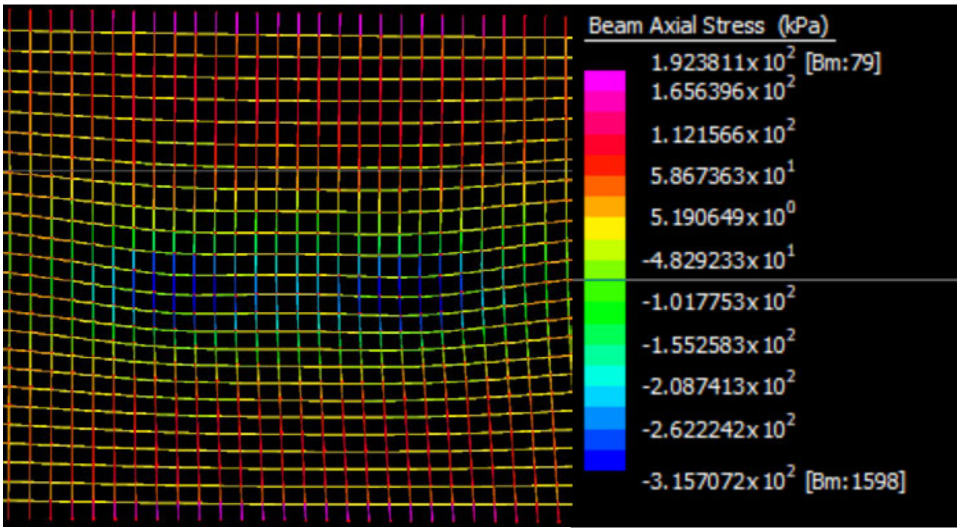

Figure 4.26: Stress distribution in slab P2

4.4. Parametric Investigation

This section will investigate the behaviour of the concrete slabs with different values of subgrade modulus, bar size and concrete compressive strength. The aim is to optimise the deflection present and improve the design.

The subgrade modulus can vary from 5000 – 300 000 kN/m^2/m dependant on soil type, compaction and if any subgrade strengthening techniques have been utilised. Table 4.1 above summarises different soil types and combinations with their corresponding subgrade modulus. The location of the approach slabs consisted of a loose sandy soil, this was then strengthened by installing a 75mm thick crushed rock layer beneath the blinder concrete. Figure 4.27 below demonstrates the behaviour of subgrade strength when compared to deflection, the red circles indicate the derived subgrade modulus value for each slab. It can be seen that the range from 50000 – 80 000 subgrade modulus has the largest impact on deflection.

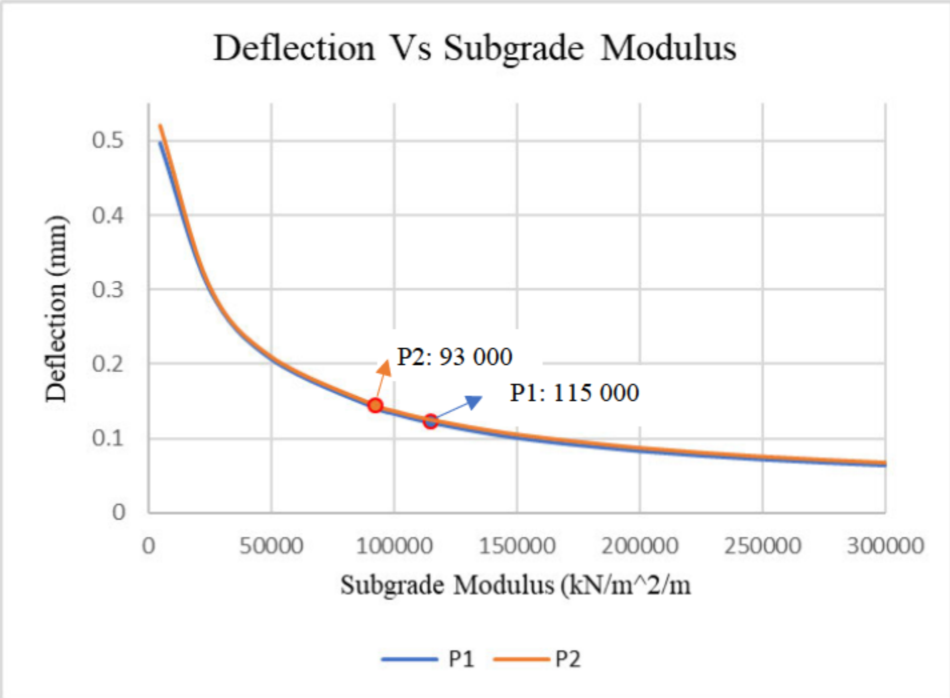

Figure 4.27: Deflection verse subgrade modulus

The variation of strain with different subgrade moduli can be seen below in figure 4.28. The red circles indicate the current subgrade modulus that was derived for each slab. This shows a similar trend to the deflection with the micro strain decreasing at a linear rate after approximately 80 000 kN/m^2/m.

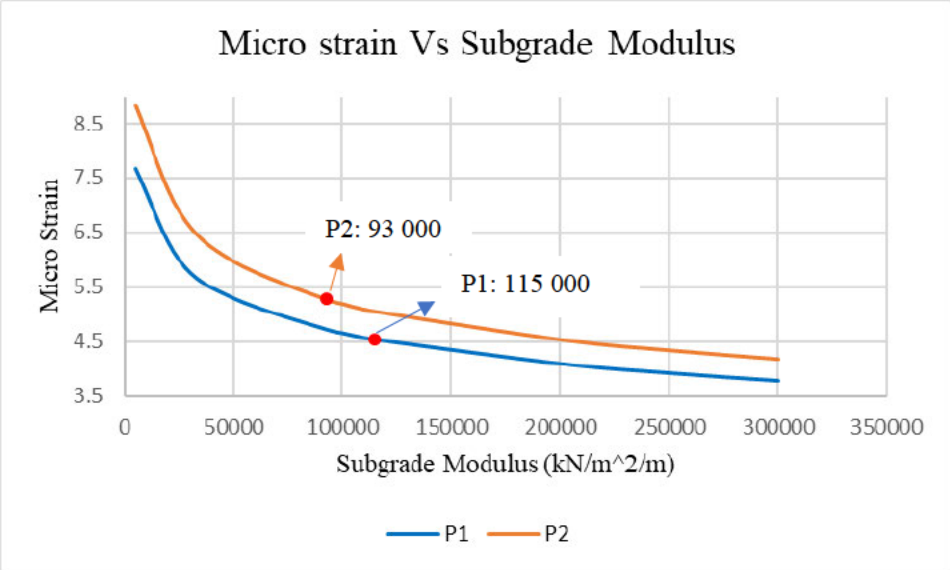

Figure 4.28: Micro strain verse subgrade modulus.

Bar size was also analysed to see the impact that this had on deflection, as shown below in figure 4.29. It can be seen that the larger spacing of reinforcement bars in slab P1 reacted better than P2 with almost no change. The small spacing in P2 showed a change in deflection of almost 0.04mm, therefore showing that bar size has only minimal effect.

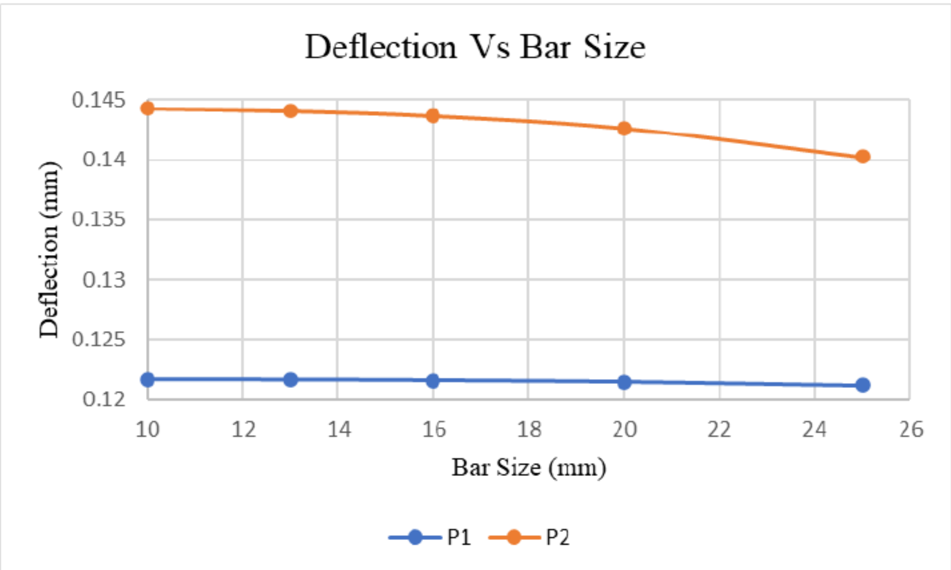

Figure 4.29: Deflection verse bar diameter

Concrete strength affected slab P2 almost 45% more when compared to P1, as shown below in figure 4.30. This demonstrates that concrete strength has slightly more effect on deflection when compared to bar diameter.

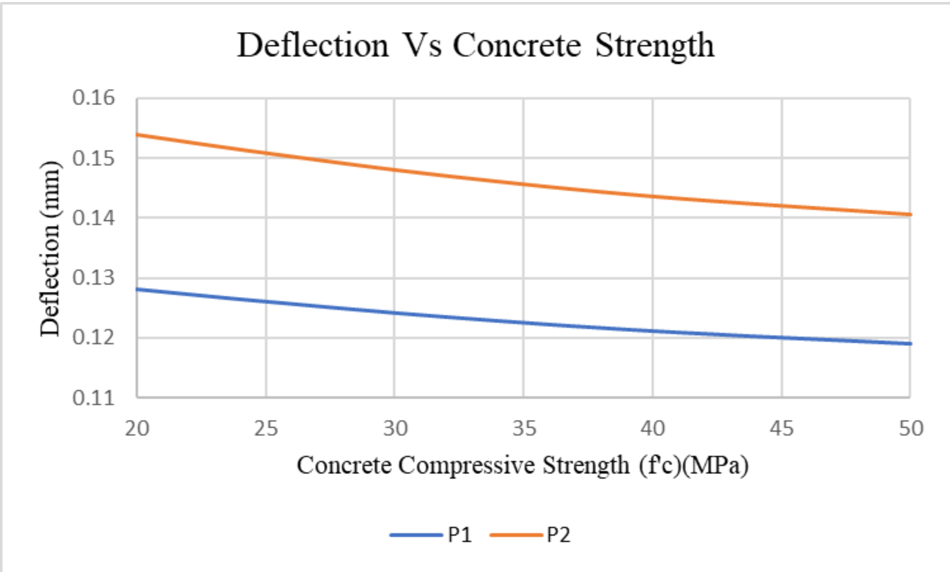

Figure 4.30: Deflection verse concrete compressive strength.

4.5. Results

The largest surface strain was recorded under dynamic loading along load path two (L_{P2}) for slab P1 showing 230 $\mu\varepsilon$. This is well under the design requirement allowing a conservative approach as concrete cracking will occur at $0.003 \times 10^6 \mu\varepsilon$. The largest strain recording within the reinforcing mesh also occurred under dynamic loading for P1 along L_{P2} with 78 $\mu\varepsilon$ also being very conservative as the ultimate rupture stain of the GFRP bars is $2.1\times 10^6\mu\varepsilon$ Benmokrane et al. (2017).

The largest deflection measured within slab P1 was 0.121 mm, this slab is reinforced with D24 GFRP bars spaced at 300 mm centres each way. This occurred under static loading as the truck was stationary on load path one (L_{P1}). The corresponding value of strain developed within the reinforcing bars was 55 micro strain. The finite element model replicated the deflection therefore deriving that the subgrade modulus was 115 000 kN/m^2/m. This soil property corresponds with crushed stone with sand in table 4.1 above (Uzodimma et al. 2020). The crushed stone sub-base layer has shown sufficient strength added to the loose sand. The finite element model derived a maximum micro strain value of 4.53, this variance shows inconclusive data and possibly faulty stain gauges. The larger spacings in slab P1 have shown to perform better when varying the material parameters, little to no change was seen in deflection while varying bar diameter. As concrete compressive strength increased, P1 showed slight improvement reducing deflection.

Slab P2 developed the largest deflection measuring 0.144 mm under dynamic loading along load path 2 (L_{P2}). P2 was reinforced with D16 GFRP bars spaced at 150 mm centres. The strain measured in the reinforcing bars was 42 micro strains, therefore slab P2 developed slightly more deflection with a lower stress value. The finite element model was able to replicate the deflection and derive that the subgrade modulus was 93 000 kN/m^2/m. This shows a slightly smaller value of subgrade strength, although this can be explained by variance in crushed rock thickness and the degree of compaction. The model showed similar results with strain, the values are slightly skewed by approximately a factor of 10. Slab P2 obtained 5.26 micro strain within the reinforcing mesh directly under the wheel load, this discrepancy is most likely caused from incorrect edge modelling within the model.

The parametric investigation discovered that the strength of subgrade modulus was the main variable when considering strain and deflection. The deflection and strain both decrease linearly as the subgrade modulus reaches 80 000 kN/m^2/m, therefore values under this are not recommended. Bar diameter, and concrete strength had very little effect on deflection within both slabs and is not considered a major concern.

The allowable deflection limit of L/800 gives a value of 5 mm as per current Australian concrete standards (Standards Association of Australia. Committee Bd-002, Concrete Structures, 2018). Therefore, deflection measured on site is under the allowable by a significant amount. This demonstrates that GFRP bars used as concrete reinforcement proves a suitable steel replacement offering small deflection rates.

Chapter 5

Conclusion and Future Work

5.1. Conclusion

Concrete is the most common building material worldwide within the construction industry. As concrete is very weak in tension the need for a reinforcing material to carry the tensile loads is required. The most common material since the 19th century is steel due to its high strength and cost effective benefits. Although steel is highly vulnerable to corrosion and rust causing major structural problems. Due to harsh marine environments most coastal bridge structures suffer from corrosion causing major repairs to be made at just 30 years of service. Concrete replacement and or repair costs the Australian economy an estimated $13 billion annually. Therefore, a more sustainable and durable material is needed especially in coastal and marine environments. Glass fibre reinforced polymer (GFRP) is becoming recognised as an alternative to steel reinforcement with its use overseas. GFRP offers various mechanical advantages when compared to steel such as increased tensile strength, one quarter lighter, non-magnetic and does not corrode. Case studies reveal 25% lower life cycle costs, increased design life, less labour and equipment while offering improved structural performance. There is currently no Australian standard for the use of GFRP therefore it is not widely used or accepted but with further results of this study it can support approval. In addition, Australian engineers and workers have very limited knowledge on the handling and construction processes of GFRP-reinforced concrete structures.

This dissertation has covered the construction of the approach concrete slabs located at the Mooloolaba boat ramp. The construction involved two different sized reinforcing bars to allow for time and motion analysis. Two slabs were constructed with D24 bars spaced at 300 mm centres each way and two slabs reinforced with D16 bars spaced at 150 mm centres. On-site loading and performance tests were then conducted to provide knowledge on how the on-ground concrete slab performs also allowing validation of a finite element model.

The time and motion investigation results were highly dependent on the skill level of the workers. This is shown as the efficiency level of the inexperienced workers range from 33 - 55% when compared to the skilled experienced workers. Tables 3.9 and 3.10 above compare experienced workers only verse all workers with the D16 and D24 reinforcement. This highlights the effect that experience workers have over the less experienced. The longitudinal retrieval and placement times would reduce, and with only minimal delays although the biggest time saving is in the tying procedure.

The D24 reinforcement only required 28 longitudinal and 44 transverse bars when compared to the D16 reinforcement needing 81 longitudinal and 87 transverse. Therefore, resulting in the D16 reinforcement requiring 1.6 times longer to construct. The D24 and D16 reinforcement required 190.7 and 309.9 worker minutes respectively. Another important observation with the D24 construction is that 2 workers were carrying 2 longitudinal bars ($\approx$11.2 kg) and one worker could carry three transverse ($\approx$15.4 kg). Previously 2 workers would be required to carry steel bars however the GFRP bars are one quarter of the weight so this practice could change and has continued simply via habit. The workers eventually adapted after laying the longitudinal as one worker continued to lay 3 transverse by themselves.

Onsite loading and performance evaluation involved loading the slab with a water truck, this delivered 10 tonnes through the rear wheels. Deflection readings were recorded with digital image correlation (DIC), which utilised a high-performance camera. Strain measurements also were recorded via strain gauges installed on the GFRP bars and surface. Results indicate very conservative levels as the highest surface strain was 230 $\mu\varepsilon$ under dynamic loading for P1 along L_{P2}. This is well under the design requirement as concrete cracking will occur at $0.003 \times 10^6 \mu\varepsilon$. The highest reinforcing mesh strain was also recorded at this position under dynamic loading which resulted in 78 $\mu\varepsilon$ also being very conservative as the ultimate rupture stain of the GFRP bars is $2.1\times 10^6 \mu\varepsilon$ Benmokrane et al. (2017).

The largest deflection of 0.144 mm recorded with in the D16 reinforced approach slab (slab P2). P1 which was reinforced with D24 bars which showed deflection of 0.121 mm, therefore showing $\approx$ 15% less deflection then P2. The finite element model developed in Strand7 software was able to derive the subgrade modulus of the supporting soil beneath the concrete slabs. The modulus of the subgrade beneath P1 was 93 000kN/m^2/m and 115 000 kN/m^2/m for P2. These values correspond to crushed stone with sand, as a 75 mm layer of crushed stone was used to stabilise the sandy subgrade. Strain measurements recorded from onsite loading show inconclusive data when compared to the finite element model. Strand7 results indicate a discrepancy by a factor of 10 within the micro strain readings, the difference is most likely caused from the edge modelling technique. The recorded values obtained onsite were 55 and 42 micro strain for P1 and P2 respectively, Strand7 results derived 4.53 and 5.26 micro strain.

The parametric investigation discovered that the strength of subgrade modulus was the main variable when considering strain and deflection. The deflection and strain both decrease linearly as the subgrade modulus increases from 80 000 kN/m^2/m, therefore values under this are not recommended. The larger spacings in slab P1 have shown to perform better when varying the material parameters, little to no change was seen in deflection while varying bar diameter. As concrete compressive strength increased, P1 showed slight improvement reducing deflection. Therefore, this study has proven that a more economical reinforcement design is to use D24 GFRP bars spaced at 300 mm centres each way.

5.2. Future Work

Based on the results of this study, GFRP is proven to perform at a high standard under loading with minimal deflection. Therefore, this shows that GFRP is a suitable material to substitute steel and further studies are encouraged to aid the acceptance into the construction industry in Australia. The following recommendations for future work are listed below.

- As the tying task consumed the most amount of time in the reinforcement construction, analysis is recommended using an automated rebar tying tool to increase production. This tool could accommodate the less experienced workers and achieve an equal or faster time then the experienced workers during the tying task.

- To improve production, it is recommended that the GFRP bars arrive onsite sorted into their corresponding lengths and diameters, as sorting the bars consumed a large amount of worker time.

- Further detailed investigation into finite element modelling, trialling different edge conditions for the slab with the aim to decrease the discrepancy within the results.

References

Abedini, M, Akhlaghi, E, Mehrmashhadi, J, Mussa, MH, Ansari, M & Momeni, T 2017, 'Evaluation of concrete structures reinforced with fiber reinforced polymers bars: A review', *Journal of Asian Scientific Research*, vol. 7, no. 5, pp. 165-75.

Alajarmeh, OS, Manalo, AC, Benmokrane, B, Vijay, PV, Ferdous, W & Mendis, P 2019, 'Novel testing and characterization of GFRP bars in compression', *Construction and Building Materials*, vol. 225, pp. 1112-26.

Benmokrane, B, Chaallal, O & Masmoudi, R 1995, 'Glass fibre reinforced plastic (GFRP) rebars for concrete structures', *Construction and Building Materials*, vol. 9, no. 6, pp. 353-64.

Benmokrane, B, Mohamed, H & Ahmed, E 2016, 'Recent developments of FRP bars as internal reinforcement in concrete structures & field applications', *4th International Conference on Sustainable Construction Materials and Technologies*, <http://www.claisse.info/2016%20papers/D168.pdf>.

Benmokrane, B, Manalo, A, Bouhet, J-C, Mohamed, K & Robert, M 2017, 'Effects of Diameter on the Durability of Glass Fiber Reinforced Polymer Bars Conditioned in Alkaline Solution', *Journal of Composites for Construction*, vol. 21, no. 5, p. 04.

Benzecry, V, Rossini, M, Morales, C, Nolan, S & Nanni, A 2021a, 'Design of Marine Dock Using Concrete Mixed with Seawater and FRP Bars', *Journal of Composites for Construction*, vol. 25, no. 1, p. 05.

Benzecry, V, Rossini, M, Morales, C, Nolan, S & Nanni, A 2021b, 'Design of Marine Dock Using Concrete Mixed with Seawater and FRP Bars', *Journal of Composites for Construction*, vol. 25, no. 1, pp. 1 - 13.

Chang, K & Seo, D 2012, 'Behavior of One-Way Concrete Slabs Reinforced with GFRP Bars', *Journal of Asian Architecture and Building Engineering*, vol. 11, no. 2, pp. 351-8.

Chu, K, Hossain, KMA & Lachemi, M 2020, 'Fatigue behavior of GFRP reinforced ECC link slabs under variable stress levels and number of cycles', *Engineering Structures*, vol. 222, p. 11.

Duo, Y, Liu, X, Liu, Y, Tafsirojjaman, T & Sabbrojjaman, M 2021, 'Environmental impact on the durability of FRP reinforcing bars', *Journal of Building Engineering*, vol. 43, p. 10.

Eduardo A Villen Salan, Muhammad K Rahman, Sami Al-Ghamdi, Jihad Sakr, Mesfer M Al-Zahrani, Antonio Nanni & JEC, EC 2021, 'A Monumental Flood Mitigation Channel in Saudi Arabia', *A Monumental Flood Mitigation Channel in Saudi Arabia*, vol. 43, no. 10, pp. 33 - 41.

Emparanza, AR, Kampmann, R, De Caso, F, Morales, C & Nanni, A 2022, 'Durability assessment of GFRP rebars in marine environments', *Construction and Building Materials*, vol. 329, pp. 1 - 13.

Gravina, RJ & Smith, ST 2008, 'Flexural behaviour of indeterminate concrete beams reinforced with FRP bars', *Engineering Structures*, vol. 30, no. 9, pp. 2370-80.

Jabbar, SA & Farid, SBH 2018, 'Replacement of steel rebars by GFRP rebars in the concrete structures', *Karbala International Journal of Modern Science*, vol. 4, no. 2, pp. 216-27.

Manalo, A, Mendis, P, Bai, Y, Jachmann, B & Sorbello, C 2021a, 'Fiber-Reinforced Polymer Bars for Concrete Structures: State-of-the-Practice in Australia, viewed on 30th August 2021', *Journal of Composites for Construction*, vol. 25, no. 1, pp. 1 - 19.

Manalo, A, Mendis, P, Bai, Y, Jachmann, B & Sorbello, C 2021b, 'Fiber reinforced polymer bars for concrete structures: state of the practice in Australia', *Journal of Composites for Construction*, vol. 25, no. 1, pp. 1 - 19.

Manalo, AC, Alajarmeh, O, Cooper, D, Sorbello, CD, Weerakoon, SZ & Benmokrane, B 2020a, 'Manufacturing and structural performance of glass-fiber-reinforced precast-concrete boat ramp planks', *Structures*, vol. 28, pp. 37-56.

Manalo, AC, Alajarmeh, O, Cooper, D, Sorbello, CD, Weerakoon, SZ & Benmokrane, B 2020b, 'Manufacturing and structural performance of glass fiber reinforced precast concrete boat ramp planks', *Structures*, vol. 28, pp. 37-56.

McCartney, D 2017, 'The problem with reinforced concrete', https://theconversation.com/the-problem-with-reinforced-concrete-56078 , viewed on 20th of march 2022>.

McCormick, N & Lord, J 2010, 'Digital Image Correlation', *Materials Today*, vol. 13, no. 12, pp. 52-4.

Nolan, S, Rossini, M, Knight, C & Nanni, A 2021, 'New directions for reinforced concrete coastal structures', *Journal of Infrastructure Preservation and Resilience*, vol. 2, no. 1, p. 1.

Ramanathan, S, Benzecry, V, Suraneni, P & Nanni, A 2021a, 'Condition assessment of concrete and glass fiber reinforced polymer (GFRP) rebar after 18 years of service life', *Case Studies in Construction Materials*, vol. 14, pp. 1-17.

Ramanathan, S, Benzecry, V, Suraneni, P & Nanni, A 2021b, 'Condition assessment of concrete and glass fiber reinforced polymer (GFRP) rebar after 18 years of service life', *Case Studies in Construction Materials*, vol. 14, p. 494.

Ruiz Emparanza, A, Kampmann, R & De Caso y Basalo, F 2017, *State-of-the-Practice of Global Manufacturing of FRP Rebar and Specifications*.

Sadraie, H, Khaloo, A & Soltani, H 2019, 'Dynamic performance of concrete slabs reinforced with steel and GFRP bars under impact loading', *Engineering Structures*, vol. 191, pp. 62-81.

Scope, C, Vogel, M & Guenther, E 2021, 'Greener, cheaper, or more sustainable: Reviewing sustainability assessments of maintenance strategies of concrete structures', *Sustainable Production and Consumption*, vol. 26, pp. 838-58.

Tekle, B, Khennane, A & Kayali, O 2017, 'Bond behaviour of GFRP reinforced geopolymer cement concrete', *MATEC Web of Conferences*, vol. 120, p. 04002.

Uzodimma, U, Nwaiwu, CMO, Obiora, J & Mezie, E 2020, 'Effect of soil compressibility on the structural response of box culverts using finite element approach', *Nigerian Journal of Technology*, vol. 39, pp. 42-51.

Wiater, A & Siwowski, T 2020, 'Comparison of Tensile Properties of Glass Fibre Reinforced Polymer Rebars by Testing According to Various Standards', *Materials*, vol. 13, no. 18.

Xu, ASaA 2016, 'Realising 100 year Bridge Design Life in an Aggressive Environment: review of the Literature', p. 137.

Yan, F, Lin, Z & Yang, M 2016, 'Bond mechanism and bond strength of GFRP bars to concrete: A review', *Composites Part B: Engineering*, vol. 98, pp. 56-69.

You, Y-J, Park, K-T, Seo, D-W & Hwang, J-H 2015, 'Tensile Strength of GFRP Reinforcing Bars with Hollow Section', *Advances in Materials Science and Engineering*, vol. 2015, pp. 1 - 8.

Appendix A

Project Specification & Schedule

ENG4111/4112 Research Project

Project Specification

For: Andrew Rayner

Title: Behaviour of GFRP reinforced approach concrete slab for boat ramp

Major: Civil engineering

Supervisors: Prof Allan Manalo and Dr Omar Alajarmeh

Enrollment: ENG4111 – EXT S1, 2021

ENG4112 – EXT S2, 2021

Project Aim: This project aims to gain understanding on the construction and behaviour

of GFRP reinforced approach concrete slab for boat ramp planks.

Programme: Version 2, 1st March 2022

1. Review of literature on the current use of GFRP bars in marine infrastructure.

2. Time and motion study on the handling and installation of GFRP bars.

3. Finite element analysis of the behaviour of GFRP reinforced approach concrete slab.

4. On-site performance evaluation of the behaviour of GFRP reinforced approach concrete slab.

5. Prepare and submit a high quality dissertation.

If time and resource permit:

6. Optimal reinforcement design for GFRP reinforced approach concrete

Schedule

Phase / Activity	Semester 1: ENG4111																	Recess		Semester 2: ENG4112																	
							Recess																							Recess							
											Fri 6 May		Fri 20 May		Fri 3 June		Fri 17 June		Fri I July		Fri 15 July		Fri 29 July		Fri 12 Aug		Fri 26 Aug		Fri 9 Sep	PP2			Fri 7 Oct		Fri 21 Oct		
	1	2	3	4	5	6	7	8	9	10	11	12	13	14	15	16	17	18	19	20	21	22	23	24	25	26	27	28	29	30	31	32	33	34	35	36	37
Meeting with supervisor																																					
1. Project preperation phase																																					
1A: Approval																																					
1B: Resources																																					
1C: Literature review																																					
2. Data collection phase																																					
2A: Time and motion																																					
3. Modelling & analysis																																					
Behaviour of Concrete slab																																					
4. Prepare dissertation																																					
4A: Progress Report																																					
4B: Prepare draft dissertation												Due 25 May																									
4C: Presentation																																					
4D: Finalise																																					
4E: Submit																																					

Appendix B

Risk Management Plan

University of Southern Queensland

USQ Safety Risk Management System

Print View

Version 2.0

Safety Risk Management Plan

Risk Management Plan ID:	Status:	Current User:	Author:	Supervisor:	Approver:
RMP_2022_6726	Approve	[redacted]	[redacted]	i:0#.w|usq\manalo	i:0#.w|usq\manalo

Assessment Title:	SRMP for research project	Assessment Date:	13/03/2022
Workplace (Division/Faculty/Section):	204010 - Faculty of Health, Engineering and Sciences	Review Date:	(5 years maximum)

Approver: *Allan Manalo*	*Supervisor: (for notification of Risk Assessment only)* *Allan Manalo*

Context

DESCRIPTION:

What is the task/event/purchase/project/procedure?	Behaviour of GFRP reinforced approach concrete slab for boat ramp
Why is it being conducted?	Undergraduate Dissertation
Where is it being conducted?	Sunshine coast, Queensland
Course code (if applicable)	ENG4111 — Chemical Name (if applicable)

WHAT ARE THE NOMINAL CONDITIONS?

Personnel involved	Andrew Rayner
Equipment	Computer
Environment	Office
Other	
Briefly explain the procedure/process	Data analysis and thesis writing

Assessment Team - who is conducting the assessment?

Assessor(s):	Belal Yousif
Others consulted: (eg elected health and safety representative, other personnel exposed to risks)	

Risk Matrix

Probability	Insignificant No Injury 0-$5K	Minor First Aid $5K-$50K	Moderate Med Treatment $50K-$100K	Major Serious Injury $100K-$250K	Catastrophic Death More than $250K
Almost Certain 1 in 2	M	H	E	E	E
Likely 1 in 100	M	H	H	E	E
Possible 1 in 1,000	L	M	H	H	H
Unlikely 1 in 10,000	L	L	M	M	M
Rare 1 in 1,000,000	L	L	L	L	L

(Consequence spans the five consequence columns.)

Recommended Action Guide

Extreme:	E= Extreme Risk – Task ***MUST NOT*** proceed
High:	H = High Risk – Special Procedures Required (Contact USQSafe) Approval by VC only
Medium:	M= Medium Risk - A Risk Management Plan/Safe Work Method Statement is required
Low:	L= Low Risk - Manage by routine procedures.

Risk Register and Analysis

Step 1	Step 2	Step 2a	Step 2b	Step 3	Step 4

Risk Register and Analysis

	Hazards: From step 1 or more if identified (Step 1)	The Risk: What can happen if exposed to the hazard without existing controls in place? (Step 2)	Consequence: What is the harm that can be caused by the hazard without existing controls in place? (Step 2a)	Existing Controls: What are the existing controls that are already in place? (Step 2b)	Risk Assessment: Consequence x Probability = Risk (Step 3)			Additional Controls: Enter additional controls if required to reduce the risk level	Risk assessment with additional controls: (Step 4) Has the consequence or probability changed?			
					Probability	Risk Level	ALARP		Consequence	Probability	Risk Level	ALARP
1	Working with...	Electrocution	Catastrophic	Check for damaged leads on a regular basis	Rare	Low						
2	Eye exposure...	Head aches, eye strain	Insignificant	Take regular breaks	Unlikely	Low						
3	Improper po...	Back pain	Insignificant	Take regular breaks and stretch	Unlikely	Low						

Step 5 - Action Plan (for controls not already in place)

	Additional Controls:	Exclude from Action Plan: (repeated control)	Resources:	Persons Responsible:	Proposed Implementation Date:

Supporting Attachments

No file attached

Step 6 – Request Approval

Drafters Name: *Andrew Rayner*

Draft Date: *13/03/2022*

Drafters Comments: *Data collection is already completed so risks are minimal*

Assessment Approval: **All risks are marked as ALARP** 0

Maximum Residual Risk Level: **Low - Manager/Supervisor Approval Required** 1

Document Status: *Approve*

Step 6 – Approval

Approvers Name: *Allan Manalo*

Approvers Position Title:

Approvers Comments: *This is approved. Andrew's remaining works are data analysis and interpretation, and mostly he will be working in his home PC.*

I am satisfied that the risks are as low as reasonably practicable and that the resources required will be provided.

Approval Decision: Approve

Approve / Reject Date: 13/03/2022

Document Status: *Approve*

Appendix C

Strand7 Results

Title: D24 Reinforcement Slab	
Project:	
Author:	Reference:

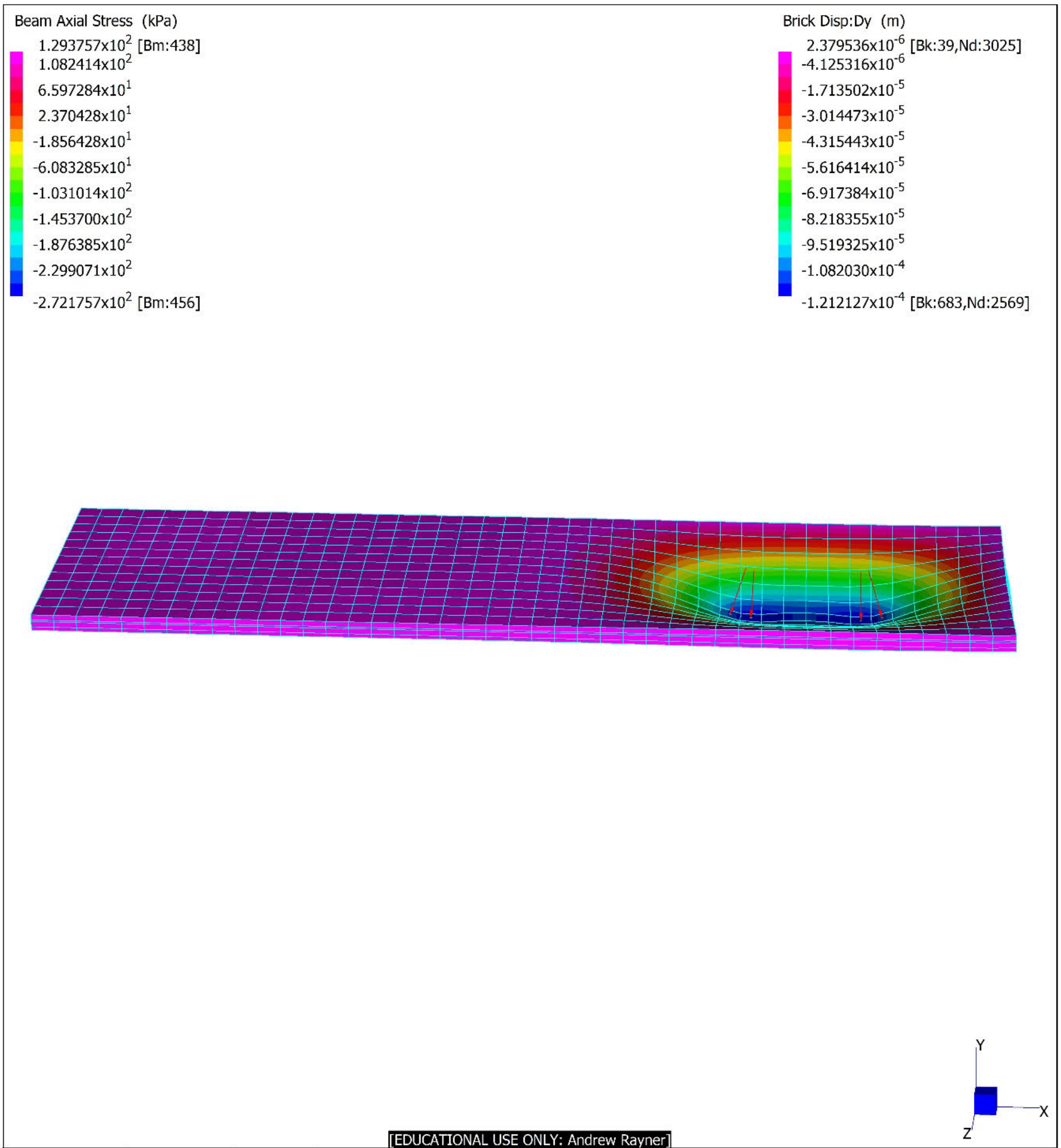

3080 Nodes 1062 Beams 0 Plates 2236 Bricks 0 Links 0 Paths	0 Vertices 0 Edges 0 Loops 0 Faces 0 Surfaces	View RX: 22.2 RY: -3.6 RZ: 0.1	7: P1-Lp1-Middle 1: Freedom Case 1 Scale: 5.0 %

Strand7 R2.4.6 [EDUCATIONAL USE ONLY: Andrew Rayner]
Model file: C:\Users\a_ray\OneDrive\Documents\Andy Uni\ENG 4111 Research Project Part 1\Slab model\300x300 New model.st7
Result file: C:\Users\a_ray\OneDrive\Documents\Andy Uni\ENG 4111 Research Project Part 1\Slab model\300x300 New model.LSA
4 August 2022 3:35 pm

Page 1

Title: D24 Mesh	
Project:	
Author:	Reference:

Beam Axial Stress (kPa)

- 1.293757×10^{2} [Bm:438]
- 1.082414×10^{2}
- 6.597284×10^{1}
- 2.370428×10^{1}
- -1.856428×10^{1}
- -6.083285×10^{1}
- -1.031014×10^{2}
- -1.453700×10^{2}
- -1.876385×10^{2}
- -2.299071×10^{2}
- -2.721757×10^{2} [Bm:456]

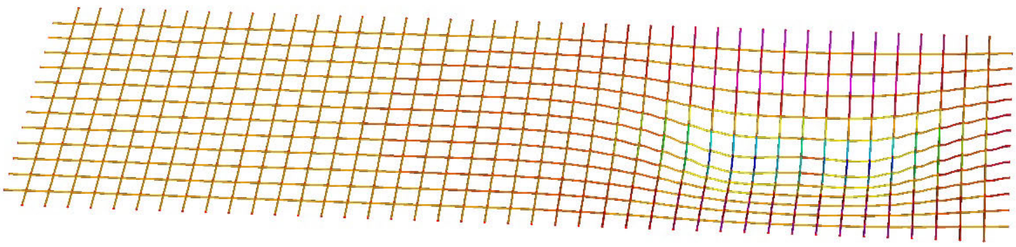

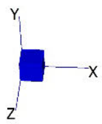

3080 Nodes 1062 Beams 0 Plates 2236 Bricks 0 Links 0 Paths	0 Vertices 0 Edges 0 Loops 0 Faces 0 Surfaces	View RX: 42.5 RY: -6.1 RZ: 2.9	7: P1-Lp1-Middle 1: Freedom Case 1 Scale: 5.0 %

Strand7 R2.4.6 [EDUCATIONAL USE ONLY: Andrew Rayner]
Model file: C:\Users\a_ray\OneDrive\Documents\Andy Uni\ENG 4111 Research Project Part 1\Slab model\300x300 New model.st7
Result file: C:\Users\a_ray\OneDrive\Documents\Andy Uni\ENG 4111 Research Project Part 1\Slab model\300x300 New model.LSA
4 August 2022 3:46 pm

Page 1

Title: D16 Reinforced Slab	
Project:	
Author:	Reference:

Beam Axial Stress (kPa)

1.923811x10^{2} [Bm:79]
1.656396x10^{2}
1.121566x10^{2}
5.867363x10^{1}
5.190649x10^{0}
-4.829233x10^{1}
-1.017753x10^{2}
-1.552583x10^{2}
-2.087413x10^{2}
-2.622242x10^{2}
-3.157072x10^{2} [Bm:1598]

Brick Disp:Dy (m)

1.431735x10^{-6} [Bk:715,Nd:3335]
-6.203254x10^{-6}
-2.147323x10^{-5}
-3.674321x10^{-5}
-5.201319x10^{-5}
-6.728316x10^{-5}
-8.255314x10^{-5}
-9.782312x10^{-5}
-1.130931x10^{-4}
-1.283631x10^{-4}
-1.436331x10^{-4} [Bk:5811,Nd:6818]

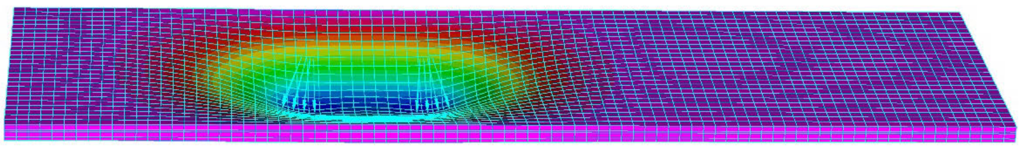

Y Z X

[EDUCATIONAL USE ONLY: Andrew Rayner]

11745 Nodes 4360 Beams 0 Plates 8944 Bricks 0 Links 0 Paths	0 Vertices 0 Edges 0 Loops 0 Faces 0 Surfaces	View RX: -156.9 RY: -4.7 RZ: -177.8	8: P2 - Lp2 - Middle 1: Freedom Case 1 Scale: 5.0 %

Strand7 R2.4.6 [EDUCATIONAL USE ONLY: Andrew Rayner]
Model file: C:\Users\a_ray\OneDrive\Documents\Andy Uni\ENG 4111 Research Project Part 1\Slab model\150x150.st7
Result file: C:\Users\a_ray\OneDrive\Documents\Andy Uni\ENG 4111 Research Project Part 1\Slab model\150x150.LSA
4 August 2022 8:56 pm

Page 1

Title: D16 Mesh	
Project:	
Author:	Reference:

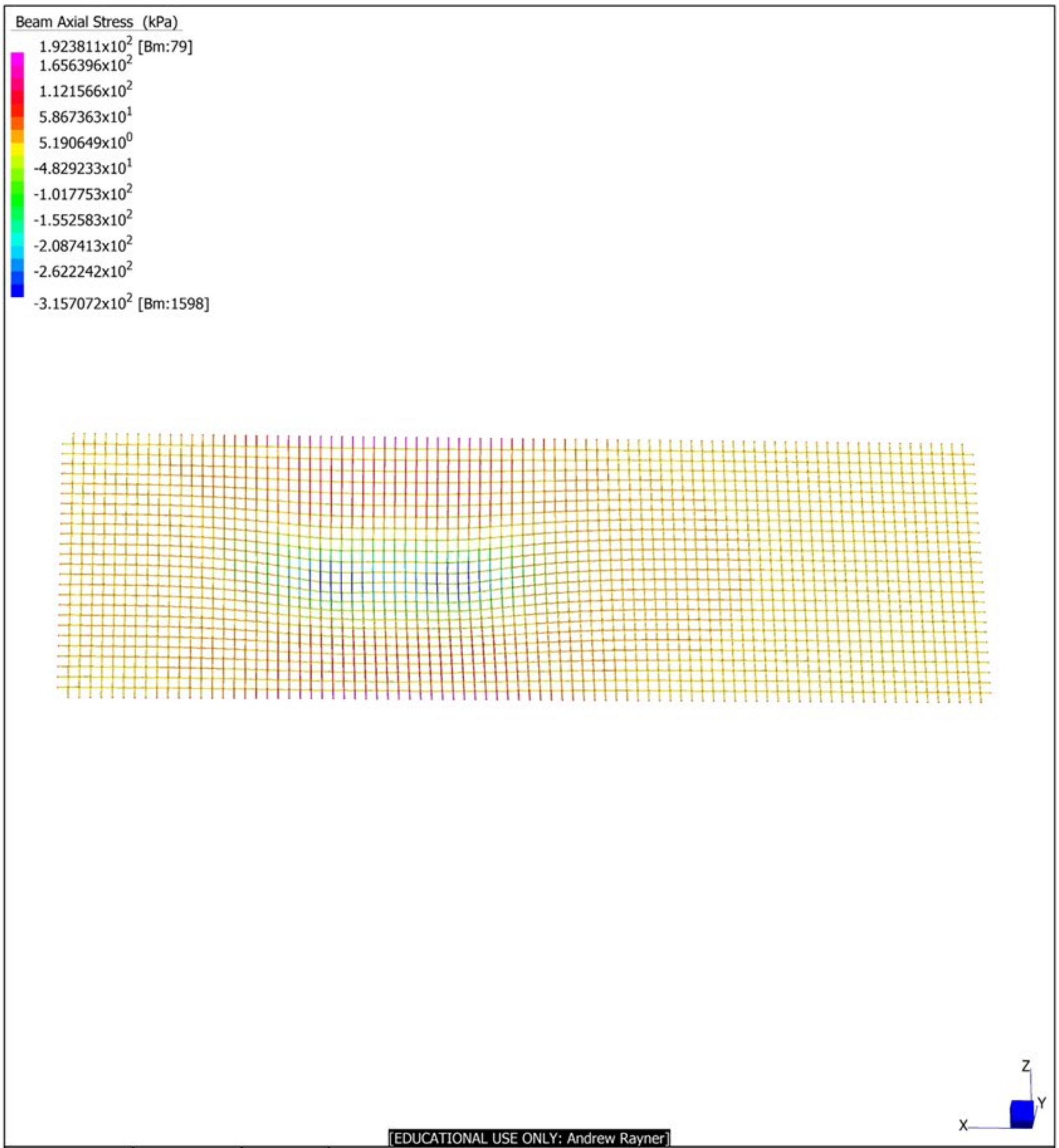

11745 Nodes 4360 Beams 0 Plates 8944 Bricks 0 Links 0 Paths	0 Vertices 0 Edges 0 Loops 0 Faces 0 Surfaces	View RX: -111.1 RY: -1.4 RZ: -174.9	8: P2 - Lp2 - Middle 1: Freedom Case 1 Scale: 5.0 %

Strand7 R2.4.6 [EDUCATIONAL USE ONLY: Andrew Rayner]
Model file: C:\Users\a_ray\OneDrive\Documents\Andy Uni\ENG 4111 Research Project Part 1\Slab model\150x150.st7
Result file: C:\Users\a_ray\OneDrive\Documents\Andy Uni\ENG 4111 Research Project Part 1\Slab model\150x150.LSA
4 August 2022 8:58 pm

Page 1